PD CF 0303

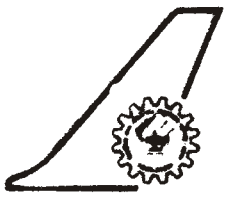

National
Aerospace
Laboratories

Free Convection in a Three-Dimensional Cavity

M D DESHPANDE
Computational & Theoretical Fluid Dynamics Division

Project Document CF 0303

June 2003
Bangalore 560 017, India

Free Convection in a Three-Dimensional Cavity

1. Introduction

Heat transfer due to the simultaneous effect of forced convection and natural convection is referred to as mixed convection. This occurs frequently in many engineering problems. Jaluria (2001) lists many traditional and new areas of material processing where fluid flow plays a critical role in quality control. These flows are very complex and we list some of the complexities relevant here being complicated geometries, multiple regions, combined mechanisms and complex boundary conditions.

We will consider the fluid motion in a rectangular parallelepiped. Since our goal is to consider both forced and free convection the governing equations, boundary conditions and the computer program are written for such a general case. But the study in this report is restricted to the natural or free convection without considering any forcing fluid motion. The transition to unsteady natural convection in a three-dimensional cavity is studied by integrating the Navier-Stokes equations with the Boussinesq approximation. The purpose of this report is to give details of the computer program and to make sure that the results obtained for the restricted free convection cases are reliable. We will see that some of the classical results to determine the critical Rayleigh number from stability theory will be obtained from the present computer program.

There have been many interesting studies regarding natural convection in two and three-dimensional cavities. Paolucci and Chenoweth (1989) investigated numerically the transition from laminar to chaotic flow in a two-dimensional cavity. They obtained the critical Rayleigh number as a function of aspect ratio. Le Quere(1990) considered natural convection in a tall rectangular cavity with differentially heated side walls. For the case of adiabatic top and bottom walls, the critical Rayleigh number was found to be 30 times larger than the corresponding perfectly conducting walls case. Janssen & Henkes (1995) studied the effect of the Prantdl number on the instability mechanism in a differentially heated square cavity for flow transition from laminar to turbulant flow. They identified one of the instabilities to be Kelvin-Helmholtz-type and also made a distinction between the instability that occurs on a vertical wall of the cavity and in the natural-convection boundary layer along an isolated vertical plate. Le Quere & Behnia (1998) also considered the differentially heated square cavity numerically and studied the statistics of unsteady solutions. They concluded that the internal gravity waves play an important role in the dynamics of the time-dependent solutions. Shankar, Meleskho & Nikiforovich (2002) considered mixed convection in a rectangular cavity. In the Stokes flow approximation the flow was generated by the combined action of differential wall heating and lid motion. They specially considered the eddy topology and also the relative role of lid motions on the buoyancy driven flows. Srivastava & Panigrahi studied formation of rolls in a layer of air heated from below. Their set-up was axisymmetric and they used a Mach-Zehnder interferometer to map the temperature fields. A stream function-vorticity formulation was used to make the corresponding calculations.

Buoyancy driven flows in 3-dimensional enclosures are more complex and the results for these cases are fewer. The classical Rayleigh-Benard cell problem is a 3-dimensional problem but is treated as a linear stability problem and has been studied extensively. A detailed account of this problem is given in Chandrasekhar(1961). Interesting accounts of this problem are given in Reid & Harris(1958, 1959), Palm(1960), Segel & Stuart(1962) and Stuart(1964). Three-dimensional numerical studies become important to address practical problems. For example, Henkes & Le Quere(1996) study the stability of flow in a square enclosure subjected to two and three-dimensional perturbations and conclude that contrary to the popular belief

three-dimensional perturbations are more unstable. Xu & Zebib (1998) consider the effect of temperature dependent surface tension but without any deformation of the flat surface. In that study the side walls were seen to suppress the flow oscillations, as expected and their effect being minimal if they are kept for apart.

2. The Mixed Convection Problem

We will formulate the problem here for mixed convection in a rectangular parallelpiped even though only the natural convection will be studied in this report.

The geometry of the contianer is shown in figure 1a. Its dimensions are l'_x, l'_y and l'_z with l'_x being measured in the vertical direction. It is filled with an incompresible, newtonian fluid of density ρ and kinematic visocity ν.

The fluid is set into motion by the diffferential heating at the walls and also by the motion of the top lid, which is assumed to move with constatnt velocity v'_0 in its own plane as shown. If $v'_0 = 0$, as will be assumed throughout in this study, we have the natural or free convection problem.

We will write down the governing equations in their non-dimensional form. The dimensional varaibles are indicated by a prime. Thus (x', y', z') are the dimensional coordinates, with x' being measured downwards as shown in figure 1a. The depth of the container l'_x, reference velocity $v'_{ref} = \nu/l'_x$ are the length and velocity scales used to non-dimensionalize. Quantities without primes are the non-dimensional variables. Hence

$$(x, y, z) = (x', y', z')/l'_x$$

$$(u, v, w) = (u', v', w')/v'_{ref} = (u', v', w')l'_x/\nu$$

$\tau = t\nu/l'^2_x$ $\qquad$ $Time$

$p = \frac{p'}{\rho v'^2_{ref}}$ $\qquad$ pressure deviation from hydrostatic pressure

$\theta = \frac{T'-T'_1}{T'_2-T'_1} = \frac{T'-T'_1}{\Delta T'}$ $\qquad$ Temperature,

where $\Delta T' = T'_2 - T'_1$ with T'_1 & T'_2 being two boundary values.

Other related variables are -

β = Coefficient of expansion = $\frac{1}{T'}$, for a perfect gas.
$\beta(T' - T'_0)$= Relative change of volume
k= Thermal conductivity
$\alpha = k/(\rho C_p)$ Thermal diffusivity
$Pr = \mu.C_P/k$ Prandtl number
$Ra = g\beta \mid T'_2 - T'_1 \mid l'^3_x/(\nu\alpha)$ Rayleigh number, with gravity g acting downward along the x-direction.

$Gr = Ra/Pr$ Grashof number
$Re_o = v_0' l_x/\nu = v_0'/v_{ref}'$ Reynolds number = speed ratio of lid.
(zero here for stationary lid).

With these variables the governing equations of continuity, momentum and energy are written with $\overrightarrow{u} = (u, v, w)$

$$D = \nabla . \overrightarrow{u} = 0 \tag{2.1}$$

$$\frac{\partial \overrightarrow{u}}{\partial \tau} + (\overrightarrow{u} . \nabla) \overrightarrow{u} = -\nabla p + \nabla^2 \overrightarrow{u} - \hat{e}_x \frac{Ra}{Pr} \theta \tag{2.2}$$

$$\frac{\partial \theta}{\partial \tau} + (\overrightarrow{u} . \nabla) \theta = \frac{1}{Pr} \nabla^2 \theta. \tag{2.3}$$

We will solve a Poisson equation for pressure which is derived by taking the divergence of equation (2.2) -

$$\nabla^2 p = -\frac{\partial D}{\partial \tau} - \nabla . [(\overrightarrow{u} . \nabla) \overrightarrow{u}] + \nabla^2 D - \frac{Ra}{Pr} \frac{\partial \theta}{\partial x}. \tag{2.4}$$

In equation(2.4), $D = 0$ but it is retained for stability reasons(see Harlow & Welch(1965)). Its value is monitored throughout the numerical solution to make sure it is indeed very small.

The boundary conditions are to be applied on all six faces for u, v, w and θ. For the case of solid walls we apply the usual no-slip boundary conditions for velocity which amount to zero value for each component on all six faces except that $v = v_0$ on the sliding top at $x = 0$. For the natural convection problem we have $v_0' = 0$. For those cases where we do not have a solid wall but a periodic boundary condition is required due to the presence of periodic cells, the normal gradient of tangential velocity component is set to zero. Similarly for temperature θ, either its value is specified or its normal derivative is set to zero in case of an insulated face. The boundary condition for p is applied numerically by solving the normal momentum equation. This will be discussed later.

Since these boundary conditions are applied numerically on a staggered grid a careful consideration is needed. This will be discussed in great detail.

3. The Staggered Grid

A cartesian grid is the natural choice for the simple geometry under consideration. Further, a uniform grid spacing is chosen in each direction with constant grid spacing Δx, Δy, Δz. This makes computer programming simpler and more importantly the numerical solution more accurate. The Marker and Cell (MAC) method and the staggered grid as proposed by Harlow & Welch (1965) are used with certain modifications. An important improvement is the adoption of a third order upwind scheme suggested by Kawamura & Kuwahara(1986) to get the finite difference analogue of the convective terms in equations 2.2 & 2.3. This scheme has good stability characteristics and maintains at the same time third order accuracy (see

Deshpande 1992). This scheme needs a five point stencil and hence special care has to be taken near the boundary.

In the staggered grid arrangment, the pressure and temperature are stored at the cell centre and at the centre of each face of the cell is specified the velocity component normal to the face (see figure 1b). The cell faces are shown by continuous lines and the mid-planes are shown by the dotted lines. The grid is extended beyond each wall to take care of the boundary conditions with the five-point stencil.

Since the fractional indices create problems we use a set of two indices in each direction. For example, along x-direction, indices i and ii are used for cell centres and faces, respectively. Similarly (j, jj) and (k, kk) indices are used along y and z directions, respectively. Now the dependent variables in the present problem will have indices as follows: $u(ii, j, k),\ v(i, jj, k),\ w(i, j, kk),\ p(i, j, k),\ \theta(i, j, k)$.

4. The Finite Difference Equations

Equations 2.2 - 2.4 are solved by a finite difference method. Equations 2.2 & 2.3 are solved by time marching using the Euler explicit method and equation 2.4 is solved iteratively for p. We will give the details of the solution procedure for the x-component of momentum:

$$\frac{\partial u}{\partial \tau} + (u\frac{\partial u}{\partial x} + v\frac{\partial u}{\partial y} + w\frac{\partial u}{\partial z}) = -\frac{\partial p}{\partial x} + \frac{1}{Re}\left[\frac{\partial^2 u}{\partial x^2} + \frac{\partial^2 u}{\partial y^2} + \frac{\partial^2 u}{\partial z^2}\right] - \frac{Ra}{P_r}\theta. \tag{4.1}$$

Its finite difference analogue centred at the point (ii, j, k) or $(i + \frac{1}{2}, j, k)$ is

$$u^{n+1}(ii, j, k) = u^n(ii, j, k) + F^n(ii, j, k) - \frac{\Delta\tau}{\Delta x}\left[p^{n+1}(i + 1, j, k) - p^{n+1}(i, j, k)\right] \tag{4.2}$$

where

$$F^n(ii, j, k) = \Delta\tau[DIFF_x - CONV_x - BUOY]^n$$

$$DIFF_x = \frac{1}{Re}[\frac{\partial^2 u}{\partial x^2} + \frac{\partial^2 u}{\partial y^2} + \frac{\partial^2 u}{\partial z^2}] \qquad \text{at } (ii, j, k)$$

$$CONV_x = u\frac{\partial u}{\partial x} + v\frac{\partial u}{\partial y} + w\frac{\partial u}{\partial z} \qquad \text{at } (ii, j, k)$$

$$BUOY_X = \theta\frac{Ra}{Pr} \qquad \text{at } (ii, j, k).$$

Here the superscript n indicates the time level. For the diffusion term $DIFF_x$ we employ the central difference scheme. The convection term $CONV_x$ needs to be stabilized. As mentioned before a third order upwind difference scheme with a five point stencil is used to approximate the first derivative. For any scalar variable Φ with index m

$$\begin{aligned}\left(u\frac{\partial\Phi}{\partial x}\right)_m &= \frac{u_m}{12\Delta x}\Big[\Phi_{m-2}-8\Phi_{m-1}+8\Phi_{m+1}-\Phi_{m+2}\Big]+ \\ &\quad \frac{|u_m|}{12\Delta x}\Big[3\Phi_{m-2}-12\Phi_{m-1}+18\Phi_m-12\Phi_{m+1}+3\Phi_{m+2}\Big]+0(\Delta x^3).\end{aligned} \tag{4.3}$$

Notice that when $u_i < 0$, the coefficients of Φ_{i-2} to Φ_{i+2} are $(-2,\ 4,\ -18,\ 20,\ -4)$ and for $u_i > 0$ they are $(4,\ -20,\ 18,\ -4,\ 2)$. This stable scheme has the high third order accuracy. For the term $u\frac{\partial u}{\partial x}$ in eqn(4.1) m asumes the value ii and the non-differenced part of u is obtained straight away since it is defined at (ii, j, k). However, difficulties arise while evaluating $v\frac{\partial u}{\partial y}$ and $w\frac{\partial u}{\partial z}$ since v and w are not defined at this point. Hence they are obtained by the following averaging, which may bring down the accuracy to certain extent. We use

$$\overline{v}(ii,j,k) = [v(i+1,jj-1,k)+v(i+1,jj,k)+v(i,jj-1,k)+v(i,jj,k)]/4 \tag{4.4}$$

$$\overline{w}(ii,j,k) = [w(i+1,j,kk-1)+w(i+1,j,kk)+w(i,j,kk-1)+w(i,j,kk)]/4 \tag{4.5}$$

$$\overline{\theta}(ii,j,k) = [\theta(i,j,k)+\theta(i+1,j,k)]/2. \tag{4.6}$$

These expressions can be substituted in equation (4.2) to evalutate F^n and u can be updated to the time step $(n+1)$ since p^{n+1} is already known from the pressure Poisson equation. Similarly we can solve equation (2.2) for the other two velocity components v and w and the energy equation (2.3) for θ. Corresponding to the group of terms F in the x component of the momentum equation, we have G and H in the y and z components of the momentum equation and T in the energy equation.

Now we turn to the pressure equation (2.4). It is solved before updating the velocity components and temperature during each time cycle. Divergence D appearing in this equation should be zero. But when we evaluate it numerically at the cell centre (i,j,k) using the central difference scheme it will have a small value. This value will be used to stabilize the pressure equation as shown below. It is convenient to write the pressure equation (2.4) in terms of the fluxes F, G, H. Also we can write $\frac{\partial D}{\partial \tau}$ as $(D^{n+1}-D^n)/\Delta\tau$ and set $D^{n+1}=0$. Then

$$\begin{aligned}\nabla^2 p &= \frac{-\partial D}{\partial \tau} - \nabla.[(\overrightarrow{u}.\nabla)\overrightarrow{u}+\nabla^2\overrightarrow{u}] - \frac{Ra}{Pr}\frac{\partial\theta}{\partial x} \\ &= \frac{1}{\Delta\tau}[\frac{\partial F}{\partial x}+\frac{\partial G}{\partial y}+\frac{\partial H}{\partial z}+D^n].\end{aligned} \tag{4.7}$$

In this equation the buoyancy term has been absorbed in F itself. Central difference scheme is used to evaluate the Laplacian and also the first derivates but only one cell width is needed to evaluate the first derivatives.

Equation (4.7) is solved iteratively by successive point over-relexation method with the relexation parameter being 1.6. Iteration is continued till the maximum change in the value of p in the field is less then a small specified value ϵ_p.

The overall accuracy of the scheme is second order in space and first order in time provided we maintain this accuracy in implementing the boundary condition.

5. Numerical Implementation of Boundary Conditions

It was mentioned earlier that the boundary conditions are known exactly and can be applied numerically. But the staggered grid leads to some problems since all the variables will not be defined on the boundaries no matter how we arrange the cells in the neighbourhood of the boundaries. We will make the cell boundaries to coincide with the computational boundaries so that the normal component of velocity is defined there. Tangential components of velocity, pressure and temperature are not defined on any boundary. To overcome this difficulty fictitious grid points are taken outside the computational domain. The values at these points are defined in such a way that the proper boundary conditions are recovered if we interpolate between the interior and the fictitious grid points. We will show some representative cases of implementation of boundary conditions below.

Second order accuracy is maintained in the numerical application so that global second order accuracy in space is maintained.

5.1. Velocity Boundary Conditions

Top Plane $x = 0$

This boundary corresponds to $i = 2\frac{1}{2}$ and $ii = 2$ and there are $1\frac{1}{2}$ grid cells beyond this boundary. On this surface normal velocity u is defined to be zero. We also need $u(ii = 1, j, k)$ which is obtained from the continuity equation to be

$$u(ii = 1, j, k) \;=\; u(ii = 3, j, k).$$

The tangential components v and w are known on this wall from the boudnary conditions but are not defined in the staggered grid arrangement. We derive the second order formulas by fitting a parabola. They are

$$v(2, jj, k) = [8Re_o + v(4, jj, k) - 6v(3, jj, k)]/3$$

$$v(1, jj, k) = [8Re_o + 2v(4, jj, k) - 9v(3, jj, k)]$$

$$w(2, j, kk) = [w(4, j, kk) - 6w(3, j, kk)]/3$$

$$w(1, j, kk) = [2w(4, j, kk) - 9w(3, j, kk)].$$

Side Wall $y = 0$

This boundary corresponds to $jj = 2$. We list the velocity boundary conditions:

$$u(ii, j = 2, k) = [u(ii, 4, k) - 6u(ii, 3, k)]/3$$

$$u(ii, j = 1, k) = [2u(ii, 4, k) - 9u(ii, 3, k)]$$

$$v(i, jj = 2, k) = 0$$

$$v(i, jj = 1, k) = v(i, 3, k), \qquad (\text{from } \nabla.\overrightarrow{u} = 0),$$

$$w(i, j = 2, kk) = [w(i, 4, kk) - 6w(i, 3, kk)]/3.0$$

$$w(i, j = 1, kk) = [2w(i, 4, kk) - 9w(i, 3, kk)].$$

5.2. Pressure Boundary Conditions

In the presence of a solid wall the momentum equation and the no-slip condition are used to derive the boundary condition for pressure. At the top wall ii=2 the momentum equation simplifies to

$$\frac{\partial p}{\partial x} = \frac{\partial^2 u}{\partial x^2} - \frac{Ra}{Pr}\theta.$$

This will give in the finite difference approximation

$$p(2,j,k) = p(3,j,k) - \frac{2}{\Delta x}u(3,j,k) + \frac{\Delta x}{2}\frac{Ra}{Pr}\Big[\theta(3,j,k) + \theta(2,j,k)\Big].$$

In case of a free surface we cannot assume no-slip condition. Hence we start with the momentum equation, again at the top wall ii=2

$$\frac{u^{n+1}-u^n}{\Delta\tau} = \frac{F^n}{\Delta\tau} - \frac{1}{\Delta x}\Big[p^{n+1}(i+1,j,k) - p^{n+1}(i,j,k)\Big].$$

This will give

$$p(2,j,k) = p(3,j,k) - \frac{\Delta x}{\Delta\tau}\Big[F(2,j,k) - \Delta u(2,j,k)\Big].$$

For the no-slip case $\Delta u = u^{n+1} - u^n = 0$ and the two expressions we have for $p(2,j,k)$ are equivalent numerically also.

5.3. Temperature Boundary Conditions

The temperature boundary condition is specified at the wall but $\theta(i,j,k)$ is not specified at the wall. For the Dirichlet-type condition let θ_0 be the wall temperature specified. Then we derive the second order boundary conditions-

$$\theta(2,j,k) = [8\theta_0 + \theta(4,j,k) - 6\theta(3,j,k)]/3$$

$$\theta(1,j,k) = [8\theta_0 + 2\theta(4,j,k) - 9\theta(3,j,k)].$$

For the adiabatic boundary condition-

$$\theta(2,j,k) = \theta(3,j,k)$$

$$\theta(1,j,k) = \theta(4,j,k).$$

5.4. Initial Conditions

For many problems in this study zero initial velocity conditions are applied. Initial value of temperature is usually taken by linear interpolation between the boundary values. In some problems values from a previous run are taken as the initial conditions.

We are now in a position to solve the governing equations since all the relevant information required to solve the finite difference equations is available.

6. Results and Discussion

As mentioned before only examples of natural or free convection will be considered in this study even though the governing equations listed and the computer program are for the more general case of mixed convecton. This is done by choosing $Re = 0$. Some special cases will be considered to establish the validity of the present numerical procedure and also to check its accuracy. Naturally the cases where standard results are known will be selected. The following cases have been considered:

Case A: Layer bounded by two rigid surfaces and heated from below.
Case B: Layer bounded by two free surfaces and heated from below.
Case C: A cubical box heated from below. Four side walls and top wall at zero temperature.
Case D: A cubical box heated from top. Four side walls and bottom wall at zero temperture.
Case E: A box heated and cooled symmetrically from two side walls. Other four walls kept at zero temperature.

The cases A and B here are the classical Rayleigh-Benard problems with critical Rayleigh numbers for them being 1707.762 and 657.511, respectively. This means that for Ra less than these values there will not be any motion even though heating is from below.

Several tests were conducted to make sure that the parameters taken in the numerical solution were satifactory. Three such parameters need to be examined and they are $\Delta\tau$, ϵ_p and the grid. We cannot possibly test each run for these parameters. What is done is to check for some cases that are somewhat more demanding. The value of $\Delta\tau$ taken for case C above was 10^{-6}. Additional test runs were made with increased $\Delta\tau$. For the case of $Ra = 10^4$, $\Delta\tau$ was increased to 10^{-5} and for the case of $Ra = 10^5$ it was increased to $5\text{x}10^{-5}$. In either case there was no significant changes in the values as functions of time indicating that the vlaue of $\Delta\tau = 10^{-6}$ is satisfactory to attain time accurate solutions. Similar tests were done for case E also. Several tests were done with ϵ_p to make sure that the convergence of the pressure Poisson equation is good. Tests for grid need more elaborate tests and after making several tests it was decided to use a (44 x 44 x 44) grid. Results from one such study are shown in figure 2 where the x-component of velocity is plotted along the line $x = y = 0.5$ for four different grids. We see that the chosen grid with 44 points in each direction is quite satisfactory.

6.1. Case A. Layer bounded by rigid surfaces and heated from below

To solve this problem we assume periodicity in the horizontal y- and z-directions and also that rigid bounding surfaces at $x = 0$ (top) and $x = 1$ (bottom), satisfy no-slip velocity condition. Further we assume $l_y = l_z$. This amounts to assuming a square cell in the horizontal direction which is heated from below with temperature $\theta = 1$ and the top wall is kept at $\theta = 0$. The four side surfaces $y = 0$, l_y, and $z = 0$, l_z are free surfaces and insulated so that the normal temperature derivative is maintained to be zero on them.

After the pioneering work of Benard (1901) and Rayleigh (1916) (see Chandrasekhar 1961) this problem has drawn considerable attention since it explains many facets of hydrodynamic stability and is also of importance in understanding convective heat transfer in flows driven by body forces like gravity. We will also see clearly in this study the effect of boundary conditions. It is well known that if the Rayleigh number is greater than a critical value $(Ra)_{crit}$ motion sets in and hexagonal cells of definite size are formed. There has also been

interesting discussion and controversy about these cells. See, for example, Reid and Harris (1958 and 1959), Chandrasekhar (1961), Palm (1960), Segel and Stuart (1962) and Stuart (1964). We will not worry about these issues at this stage but consider the problem as a numerical test case and make some comments in a later section. The present results are in conformity with well established results.

We select Prandtl number $Pr = 0.1$ and later study for $Pr = 1$ also. It is important to realise at this stage that we are modelling a layer of fluid subjected to instability and the most disturbing wave numbers depend on the depth (=1 in this case), fluid properties and the boundary conditions. Since we are restricting ourselves to only one square cell based on periodicity, it is necessary that we should select a value for the width of this cell $l_y(= l_z)$. In principle one can figure out numerically the most disturbing wave length but it will be very expensive to search in a two parameter domain involving 3-D calculations. Hence what is done here is to select from the literature the most disturbing wave number $a = 3.117$. This will give for the square cell $\frac{2\pi}{a} = l_y = l_z = 2.0160$. Stuart (1964) discusses extensively the issue of cells and also points out the mistakes in the arguments and pictures in some of the earlier work. It was helpful in the present study to correctly choose the value of l_y.

Now we can select a value of Ra and check if there is motion or it is a static case and in principle arrive at the value of $(Ra)_{crit}$. But it is not a simple exercise. When an input value of subcritical Ra is employed the values of velocity at different points are not going to be exactly zero and one has to decide whether the small values we have are just noise during arithmetical calculations or will these small values grow in time. There are also practical problems like at which locations one has to observe velocities, how long one should continue the calculations, what should be the values for $\Delta\tau$ and ε_p in the computations and whether the observations are made after the temperature field has stabilized. Near the critical value of Ra these aspects can be tricky.

Taking $l_y = l_z = 2.0160$ and $Pr = 0.1$ several calculations were done for a wide variation of Ra and a fine resolution was aimed once the calculations appeared to be close to the critical value. Between 1706 and 1708 an increment 0.1 in Ra was used. For the case of $Pr = 0.1$ the value $Ra = 1707.5$ turned out to be just supercritical. But when the size of the square cell was changed to $l_y = l_z = 2.00$ or 2.03 a distinctly decaying motion was observed confirming that $l_y = l_z = 2.0160$ leads to a more destabilizing wave number.

The calculations were repeated with $Pr = 1$ and these led to similar results. The motion was seen to be like steady state at $Ra = 1707.5$ but with very low values and it was growing at $Ra = 1707.6$. In the light of the uncertainties, specially near the critical value it is concluded that $(Ra)_{crit} = 1707.5$ which compares favourably with the value of 1707.762 from linear stability theory.

6.2. Case B. Layer bounded by free surfaces and heated from below

This problem is treated in a way similar to case A except that the boundary conditions at the top and bottom surfaces are treated as free surfaces instead of rigid walls. Another change needs to be kept in mind if we are searching for $(Ra)_{crit}$ (which is 657.511), i.e. the value of the critical wave number changes. Hence the size of the square cell changes. Corresponding to the value of $a = 2.22144$ (see, for example, Chandrasekhar 1961) we get $l_y = l_z = 2.8284$ which was selected for the calculations in this section, unless otherwise stated.

Calculations were done for several values of Ra between 650 and 1000. In figure 3 are shown the time traces of x-component of velocity at $y = z = 0.5$ for several values of Ra, with

initial conditions obtained from computations for $Ra = 798$ and upto $\tau = 30$. For $Ra = 650$ and 655 we see a decay of velocity and for $Ra = 660,\ 665,\ 670$ and 700 there is an increased rate of growth in time. It was concluded that $(Ra)_{crit}$ was between 655 and 660 and no further attempts were made to resolve this interval.

A different exercise was done, however, for the case of $Ra = 660$. Since this value of Ra is just supercritical for the most disturbing wave numbers leading to $l_x = l_y = 2.8284$, calculations were done changing the size of the square cell to $l_y = l_z = 3.1$ in one case and to 2.6 in the other. See figure 4. With a change of Ra from 798 to 660 but keeping $l_y = l_z = 2.8284$ decreased the rate of growth of velocity u but it kept growing to instability. Change of l_y from this critical value, on the other hand, had a drastic effect at $Ra = 660$. This decrease (curve B in figure 4) and increase (curve C in figure 4) in the wave number led to stability of the flow by a gradual decrease in velocity even though the initial motion was one of growth. This was to be expected. A similar excercise for $Ra = 798$ did not damp the motion since the value of Ra now is too high compared to the critical value. See figure 5.

6.3. Comments on the cell patterns in the Rayleigh-Benard Convection

This problem has been studied by many investigators as a problem in stability. The linear stability theory is generally employed and it cannot predict the cell shape. It, however, gives the correct values for the critical Rayleigh number and the corresponding wave number. Since there is no preferred direction in a horizontal plane it is reasonable to assume that the entire plane is tesselated into regular polygons with cell walls being surfaces of symmetry. This requires that the polygons be either equilateral triangles, squares or regular hexagons (see Chandrasekhar (1961), page 43).

Hexagonal cells have been observed experimentally and attempts have been made to show that this indeed is the preferred shape. See, for example Palm (1960). Palm also concluded that the effect of the dependence of the kinematic viscosity on temperature is to lower the critical Rayleigh number and also that this dependence is the agency responsible for the preference of hexagonal shapes for the cells. It is interesting to note that the direction of flow in a hexagonal cell also is determined by the dependence of kinematic viscosity on temperature. Flow direction is indeterminate under the stability theory. Suggestions were made by Graham (see Palm 1960) in 1933 that flow direction in a hexagonal cell is in the direction of increasing kinematic viscosity. In liquid layers heated from below, it amounts to flow being upwards at the cell centres and downwards near the cell walls. For gases it is exactly the opposite since the kinematic viscosity increases with temperature. Experiments by Tippelskirsh (see again Palm 1960) with liquid sulphur verified this dependence of flow direction on the temperature dependence of kinematic viscosity. This substance has the peculiar property that its kinematic viscosity is a minimum at 153^0C and it can be first decreased and then increased by increasing the temperature around this value.

Segel and Stuart (1962) and Stuart (1964) point out the mistakes in the paper by Palm (1960) and conclude that it was not proved by Palm that hexagonal cells are the preferred shapes (even though other conclusions indicated above remain valid) but a sufficiently large variation of kinematic viscosity with temperature leads to hexagonal shapes. Further, they draw attention to the definition of a cell to be such that it is bounded in the horizontal plane by a contour through which no fluid flows and along which the vertical velocity has one sign. Stuart (1964) concludes further that based on this definition of a cell the square and rectangular arrangements described earlier in the literature as cells are not really so. He points out the kind of confusion that existed in the literature in identifying the part in

a rectangular periodic flow that is to be called a cell. He also opines that the triangular periodic flow called as a cell, for example, in Chandrasekhar (1961) is not really a cell.

In the present study we do not face these difficulties. The paper by Stuart (1964) was helpful in correctly identifying l_y and l_z based on the critical wave number. Since these values are given as inputs the question which mode is preferred does not arise. The hexagonal cell is out of question. The periodic flow we attain, when $Ra > (Ra)_{crit}$ is simply called here as a square cell. We have also shown that the critical value of Ra is predicted correctly in both the cases and this value is also sensitive to the choice of l_y and l_z. Since uniform fluid properties are assumed, the dependence of direction of vertical velocity on kinematic viscosity does not arise. The actual flow direction in the solution is chosen by the numerical procedure and no tests are doen in this regard.

6.4. Case C. A cubical box heated from below

This case differs drastically from the previous two since the temperature is specified on each wall: $\theta = 1$ at the bottom wall and $\theta = 0$ on the other five walls. No-slip velocity condition is applied on all the six walls. The temperature field here is not uniform in the horizontal plane even for the lowest values of Ra as it was in the previous two cases. This nonuniformity sets the motion even for the smallest values of Ra or temperature differences.

The range of Ra studied is from 100 to 10^6 and for three values of $Pr = 0.1,\ 1$ and 7. For the case of $Pr = 0.1$ streamlines, temperature contours and velocity and temperature profiles are shown in figure 6. In frames (a) and (b) are shown the streamlines for the case Ra=1,000. The flow has organized into eight distinct wedge shaped toroidal cells as seen along the x-direction. The flow is directed upwards near the vertical centre of the cube $y = z = 0.5$. On the outer toroidal surfaces a fluid particle generally moves towards the vertical diagonal planes $z = y$ or $z = 1 - y$. It is brought back towards the vertical planes $y = 1/2$ or $z = 1/2$ by the inside helical path. One such wedge shaped toroidal streamline contained between two planar streamlines is shown in frame (b). Four such planar streamlines on the planes $y = 0.5$ or $z = 0.5$ spiral out. The other four planar streamlines on the diagonal planes $z = y$ or $z = 1 - y$ spiral inwards as seen in frame (b). Thus these eight vertical streamsurfaces divide the cube into eight parts as seen in frame (a).

In frames 6(c) and (d) are shown the profiles of u on the line $x = z = 0.5$ and as a function of y. We see that for the four values of $Ra = 10^2,\ 10^3,\ 10^4$ and 10^5 the profiles are symmetrical in y. These are the steady state values. The transient flows till the steady state was reached also remained symmetrical in y. For the case of $Ra = 10^6$ the profile shown is at a particular instant since the flow remains unsteady and we see that this symmetry is lost. The hot plume rises at the centre pushing the cold fluid down along the vertical walls. In frame (e) are plotted y-component of velocity v on the mid x-line $y = z = 0.5$. This value is negligibly small because of symmetry upto $Ra = 10^5$ but attains a substantially large value for $Ra = 10^6$. The z-component of velocity plotted along z in frame (f) on the centreline $x = y = 0.5$ is antisymmetrical in z for the values of Ra upto 10^5. For $Ra = 10^5$ the flow on this line is toward the mid plane $z = 0.5$ except near the end planes $z = 0$ and $z = 1$ where it is directed toward them. For $Ra = 10^6$ we see again the loss of symmetry and flow remains unsteady.

The temperature profiles along x on the centreline $y = z = 0.5$ shown in frame 6(g) indicate the gradually increasing influence of the bottom plane as Ra increases. This is because of the upward flow along the vertical centreline. For $Ra = 10^5$ the effect of the top plate is localized to a shorter distance. For $Ra = 10^6$ the flow remains unsteady and the temperature

is somewhat uniform at the average value away from the top and bottom walls. Temperature contours are shown on two x-planes $x = 0.2$ and $x = 0.8$ in frame (h) and on $y = 0.5$ plane in frame (i) for $Ra = 1000$. Since the value of Ra is only moderate the effect of flow is not perceptible on these contours and the presence of the flow cells we saw in frame 6(a) is not perceptible here. At a higher Ra of 10^5, on the other hand, the flow is more vigorous and we see its effect on the streamlines in frame (j). Flow is steady and there are eight distinct cells, symmetrically placed similar to those in frame 6(a) for $Ra = 1000$. But we see that a fluid particles appear to have a more erratic motion. The temperature contours shown for this case of $Ra = 10^5$ in frame 6(k) and 6(l) clearly show the effect of motion. The temperature contours in a z-plane will be same as those in a corresponding y-plane because of symmetry and hence are not shown here.

Effect of Ra on the motion is studied in figure 7a. Scaling corresponding to $Ra = 100$ is done to the other two u profiles in figure 6c by dividing these values by 10 and 100. An increase in Ra increases velocity more than proportionately. This nonlinear effect was seen to be more for higher values of $Pr = 1$ and 7. Effect of Pr on u profiles is shown for two values of $Ra = 1000$ (figure 7b) and $Ra = 10^5$ (figure 7c). A similar study of temperature profiles along x centreline shows that Pr has no effect at a smaller value of $Ra = 10^3$ (figure 7d) but there is Pr dependence at $Ra = 10^5$ as shown in figure 7e.

6.5. Case D. A cubical box heated from top

This case is similar to case C except that the top wall of the cube is kept at $\theta = 1$ and the other five walls at $\theta = 0$. Again, no-slip boundary condition is maintained on all the six walls. It is a very surprising case since the nonuniform temperature gradient in the horizontal plane sets the motion even though it is heated from top. A comparison is made subsequently with case C where heating is from below.

In figure 8a the x-component of velocity is plotted along the y-centreline $x = z = 0.5$ for four values of $Ra = 1,\ 10,\ 100$ and 1000. It is for $Pr = 0.1$ and also the velocity is scaled by Ra for comparison with the case $Ra = 100$. The hot plume again rises at the centre of the cube. This figure should be compared with case C, figure 7a. First, the scaled down values do not vary much for Ra smaller than 100 and the values are comparable in the two cases, i.e. whether the cube is heated from top or from below. Interestingly the effect of heating from top is to reduce the effect of increased Ra as against in case C. Temperature profiles in figure 8b are seen to be less sensitive to Ra than velocity profiles.

A direct comparison between cases C and D is done in figures 9 for x-component of velocity along the y-centreline $x = z = 0.5$ and for temperature distribution along the x-centreline $y = z = 0.5$. The two cases start differing from each other as Ra increases. Temperature field, as expected, shows much less sensitivity to Ra, even though the trends are similar.

6.6. Case E. Box heated and cooled symmetrically from sides

In this case two side walls $y = 0$ and $y = l_y$ are held at temperatures $\theta = -\frac{1}{2}$ and $\frac{1}{2}$, respectively and the other four walls are at zero temperature. No-slip velocity condition is applied on all the six walls. Three values of Pr, namely 0.1, 1 and 7 are employed but we will show results for the case $Pr = 0.1$. Due to the differential heating at the walls, a circulatory motion is set in.

We see two views of this motion in figures 11a - 11d at Ra=100 and 1000. These streamlines

were obtained by releasing two particles at corresponding z points and then integrating the steady velocity field using the commercial visualisation package CFD-VIEW. This case has been studied by Shankar et al (2002) for the two dimensional case. The closed streamline patterns there may be compared with the one in figure 11a which differs even qualitatively because of three-dimensionality. The planes $z = 0.5$ and $y = 0.5$ are planes of symmetry. The two toroidal vortices are such that in the neighbourhood of their centres the fluid moves towards midplane $z = 0.5$. As Ra is increased to 10^4 (figure 11e) and then to 10^5 (figure 11f) we see that the motion appears more erratic. But still the motion is steady and symmetry about the two planes mentioned above is maintained. One can imagine that for a sufficiently high Ra such symmetry and steadiness will be lost. The temperature contours plotted in figure 12 on the $z = 0.5$ plane indicate this symmetry in y and also the enhanced propagation of the effect of hot ($y = 1$) and cold ($y = 0$) walls as Ra increases. A quantitative picture of these observations is presented in the velocity and temperature profiles in figure 13.

7. Conclusion

Natural convection in a rectangular parallelepiped due to the application of differential temperature on the walls and under the Boussinesq approximation has been studied in this report. Time accurate numerical solutions of the Navier-Stokes equations have been obtained for a variety of cases with different boundary conditions.

Two types of boundary conditions are applied for velocity - no-slip condition and the free-surface condition. For temperature it is either the Dirichlet-type with specified value or the insulated case where the normal derivative is zero. Since there are six faces one can formulate a variety of combinations. We have considered five representative cases of interest which also help in establishing the reliability of the 3-dimentional computer program.

Two cases of Rayleigh-Benard convection are taken up to check if the correct values of critical Ra and wave number can be recovered. The procedure here is different from the classical linear stability theory where the cell pattern and flow direction inside a cell remain indeterminate. In the present approach, on the other hand, we cannot handle a fluid layer of infinite extent and hence a square cell in the horizontal plane is assumed. Its size is fixed to correspond to the critical wave number given by the linear stability theory. Now the search can be done in a single parameter Ra. This procedure has many practical difficulties but has been applied successfully to evaluate $(Ra)_{crit}$ for two cases. For a case when Ra is just supercritical a change in the disturbances wave number due to the change in l_y and l_z damped the flow to a static case as expected.

Cubical box subjected to differential heating leads to instability even for the lowest value of Ra. This is true even for the case where heating is done at the top. This case is similar to the one where heating is done from below (but for the change in direction) if Ra is small. For larger values of Ra nonlinear effects show up and they are qualitatively different for these two cases. For a sufficiently large Ra the flow cannot be steady. Effect of Prandtl number also has been studied. Generally its effect is negligible if Ra is small.

The purpose of this report was to establish the reliability of the computer program by comparing the results with those available in the literature and also to run it for a variety of cases to get a feel for these problems. Internal consistency of the results and also comparison with other results indicate that this goal has been met.

I would like to thank Dr.S. Majumdar for helpful suggestions and Mr. B.G. Srinidhi, Mrs. D. Shobha, Mrs. L. Vijayalakshmi and Mr. Mallikarjun for the help in the preparation of

the manuscript.

References

1. Chandrasekhar, S. (1961) Hydrodynamic and Hydromagnetic stability. Oxford at the Clarendon Press.

2. Deshpande, M.D.(1993) Flow regimes in a three-dimensional driven cavity. NAL Project Document PD CF 9305.

3. Deshpande, M.D. (1992) Stability analysis of the third order upwind difference schemes. NAL Project Document PD CF 9214.

4. Harlow, F.H. & Welch, J.E. (1965) Numerical calculation of time-dependent viscous incompressible flow of fluid with free surface. Physics of Fluids, **8**, 2182-2189.

5. Henkes, R.A.W.M. & Le Quere, P. (1996) Three-dimensional transition of natural-convection flows. J.Fluid Mech. **319**, 281-303

6. Hirt, C.W and Harlow, F.H.(1967) A general corrective procedure for numerical solution of initial value problems. J. Comp. Phsyics, **2**, 114-119.

7. Jaluria, Y.(2001) Fluid Flow phenomena in material processing - The 2000 Freeman Scholar Lecture. J. of Fluids Engg. **123**, 173-210.

8. Janssen, R.J.A. & Henkes, R.A.W.M. (1995) Influence of Pandtl number on instability mechanisms and transition in a differentially heated square cavity. J.Fluid Mech. **290**, 319-344.

9. Kawamura, T. & Kuwahara, K. (1986) Computation of high Reynolds number flow around a circular cylinder with surface roughness, Fluid Dynamics Research, **1**, 145-162

10. Le Quere, P. & Behnia, M. (1998) From onset of unsteadiness to chaos in a differentially heated square cavity. J.Fluid Mech. **359**, 81-107

11. Le Quere, P.(1990) Transition to unsteady natural convection in a tall water-filled cavity. Physics of Fluids A,**2**, 503-515.

12. Palm, E. (1960) On the tendency towards hexagonal cells in steady convection. J.Fluid Mech. **8**, 183-192.

13. Paolucci, S. & Chenoweth, D. (1989) Transition to chaos in a differentially heated vertical cavity. J.Fluid Mech. **201**, 379-410.

14. Prasad, A.K. & Koseff, J.R (1996) Combined forced and natural convection heat transfer in a deep-lid driven cavity flow. Int.J. Heat and Fluid Flow **17**, 460-467.

15. Reid, W. H. & Harris, D. L. (1959) Streamlines in Benard convection cells. Physics of Fluids, **2**, 716-717.

16. Reid, W.H. & Harris, D.L. (1958) Some further problems on the Bernard problem. Physics of Fluids, **1**, 102-110.

17. Segel, L.A. & Stuart, J.T. (1962) On the question of the preferred mode in cellular thermal convection. J.Fluid Mech. **13**, 298-306.

18. Shankar, P.N., Meleshko, V.V. & Nikiforovich, E.I. (2002) Slow mixed convection in rectangular containers. J.Fluid Mech. **471**, 203-217.

19. Srivastava, A. & Panigrahi, P.K. (2002) A combined numerical-experimental study of convection in an axisymmetric differentially heated fluid layer. Indian Journal of Engg. & Materials Sciences, **9**, 448-454.

20. Stuart, J.T. (1964) On the cellur patterns in thermal convection. J.Fluid Mech.**18**, 481-498.

21. Xu, J. & Zebib, A. (1998) Oscillatory two and three-dimensional thermocapillary convection. J.Fluid Mech. **364**, 187-209.

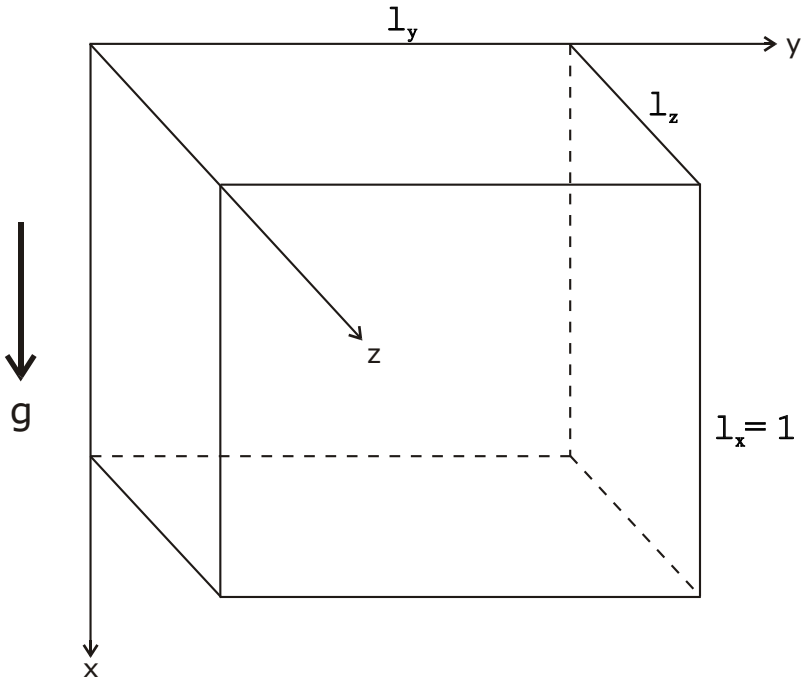

Figure 1(a) Geometry of the cavity.

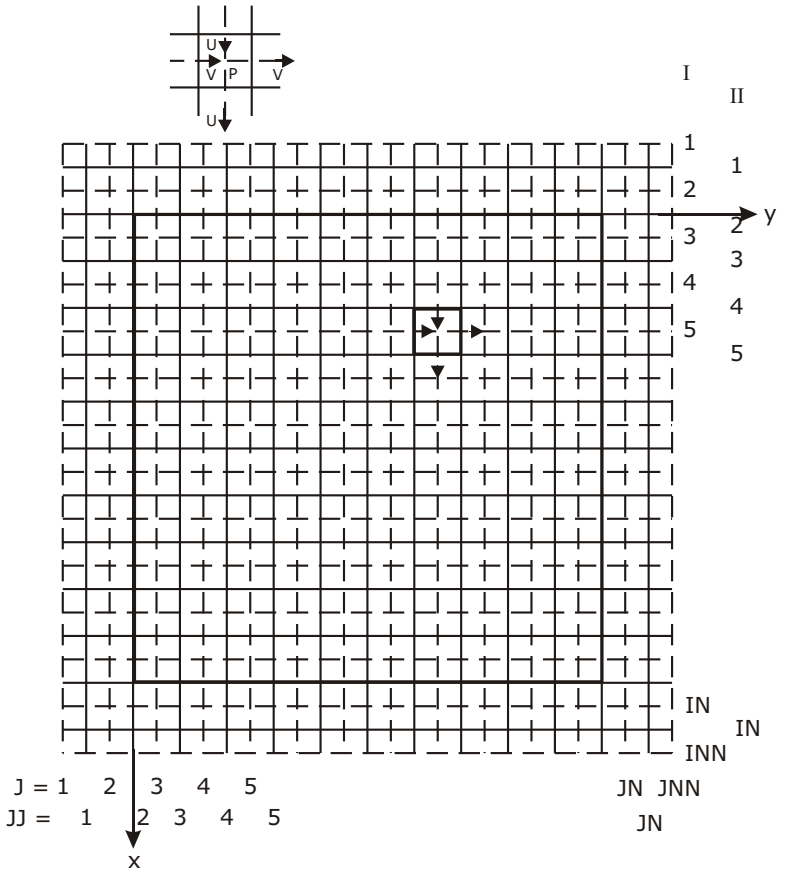

Figure 1(b) The staggered grid and specification of velocity components and pressure. The z-direction is not shown for simplicity.

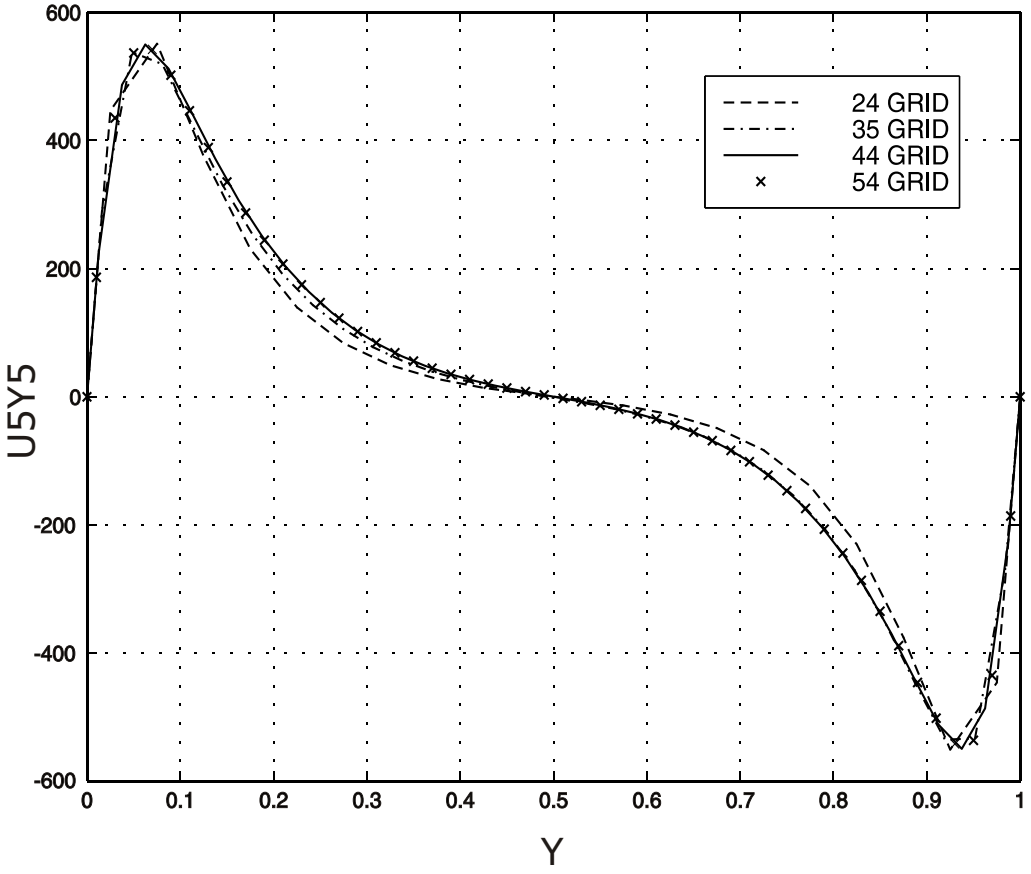

Figure 2. Grid independence study. Case E with Pr=0.1, Ra=10^5. X-component of velocity is plotted on l_x=l_z=0.5 centreline for four different grids.

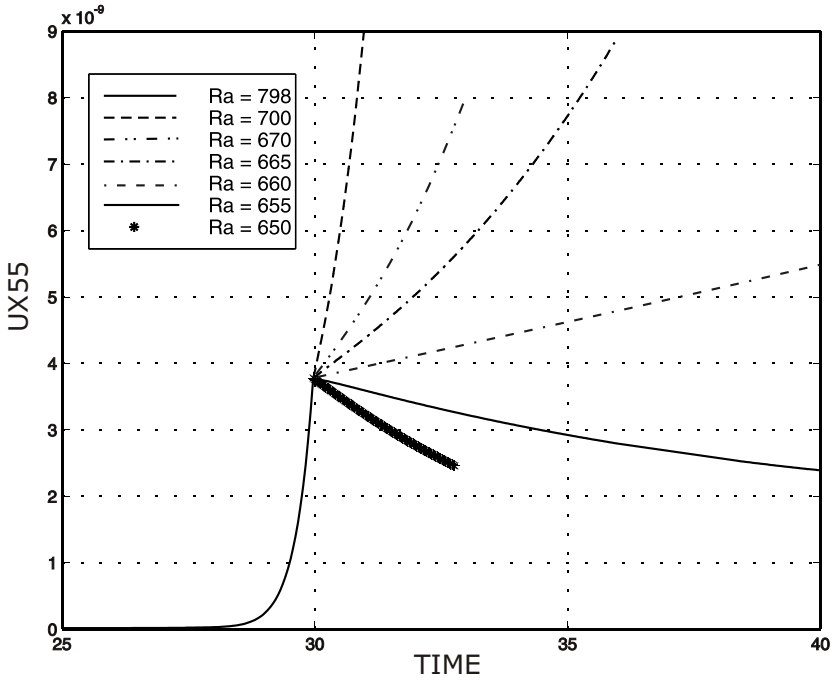

Figure 3. Time traces of *x*-component of velocity to determine critical *Ra* for case B with free-free boundaries. *Pr*=0.1. Initial conditions from supercritical *Ra*=798 are upto time = 30 units. Velocity grows for *Ra*=700, 670, 665 & 660 and decays for *Ra*=655 & 650, indicating $Ra_{(crit)}$ to be between 655 and 660.

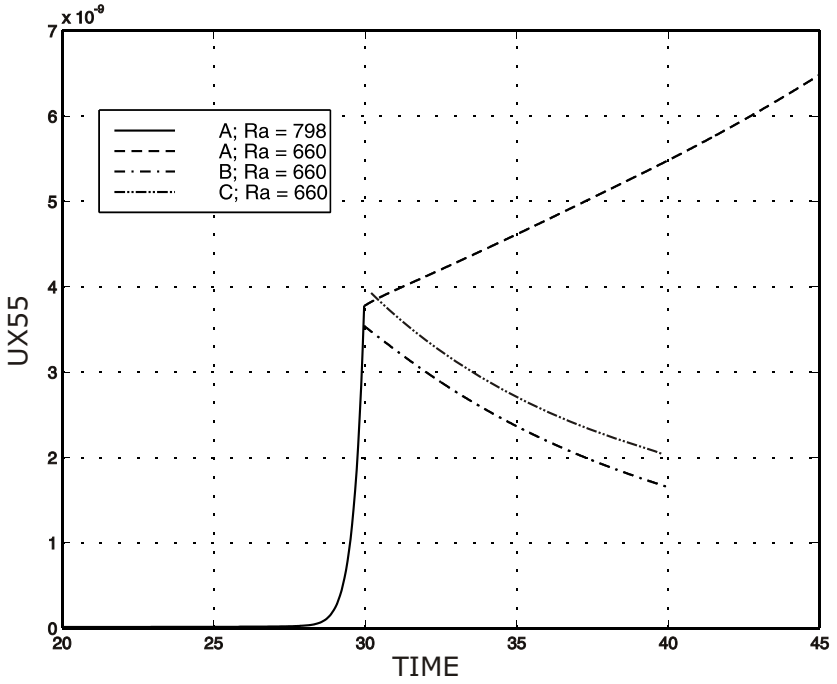

Figure 4. Similar to figure 3. For *Ra*=660 velocity *u* is growing for critical wave length l_y=2.8284 but decays for l_y=3.1(bottom descending curve B) and also for l_y=2.6 (top descending curve C).

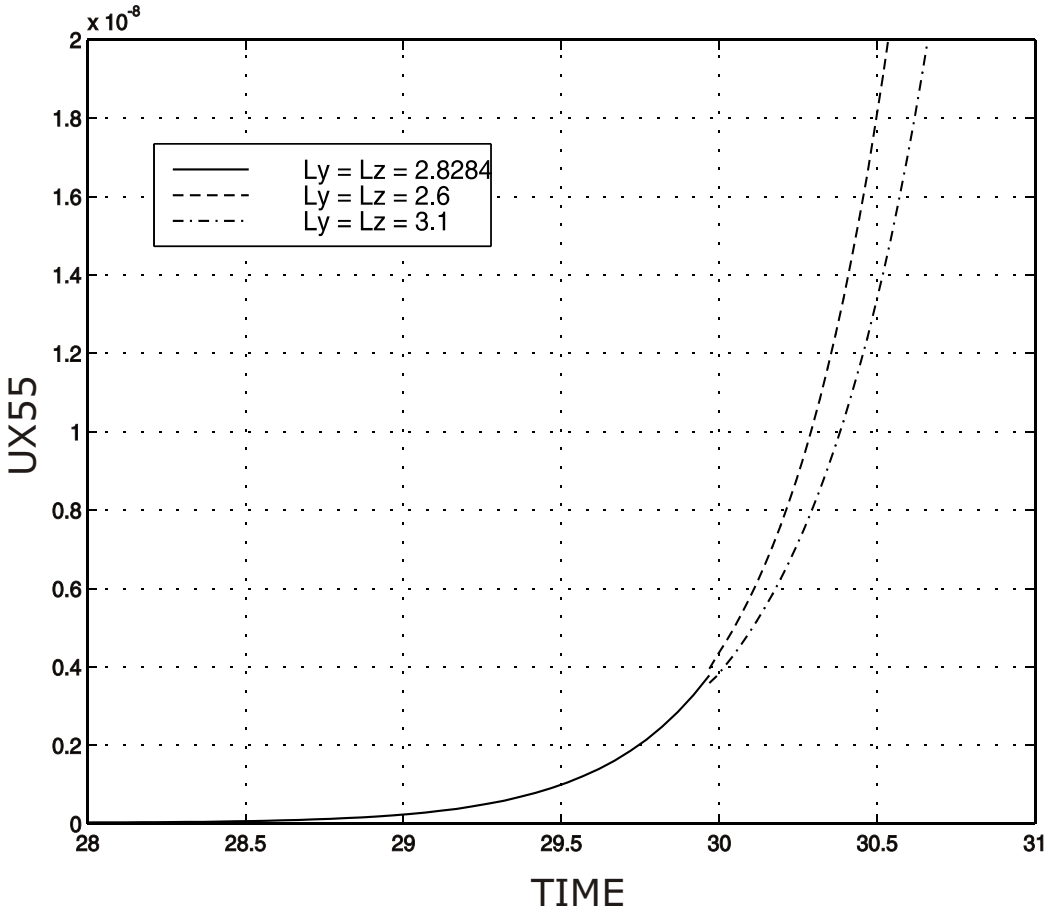

Figure 5. Similar to figure 3 but *Ra*=798 for all 3 curves. Change of l_y from the critical value of 2.8284 to 2.6 and 3.1 did not make flow stable since *Ra* is too high compared to $(Ra)_{(crit)}$.

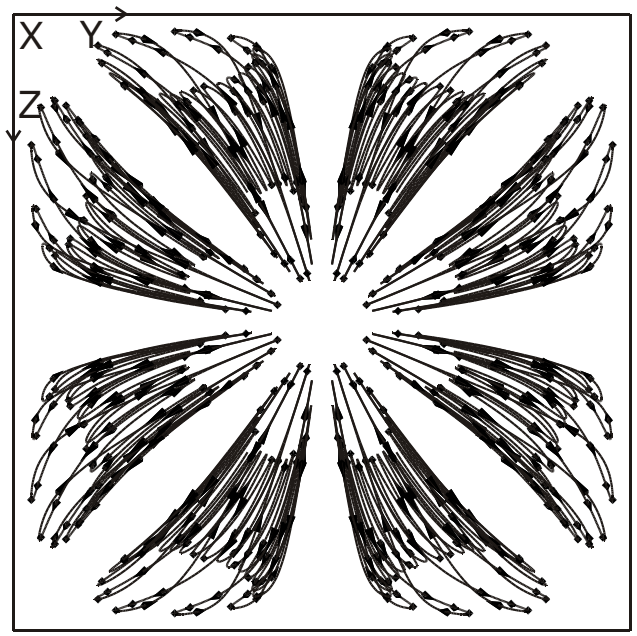

Figure 6. Case C, cubical cavity heated from below. *Pr*=0.1.
(a) Streamlines in top view along *x*-axis, *Ra*=1000.

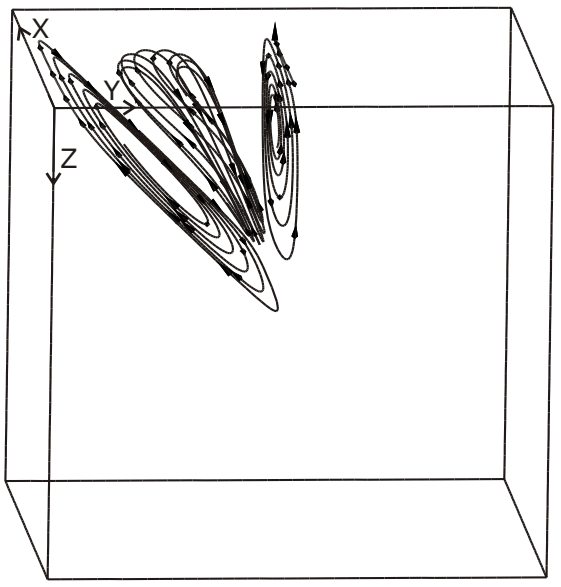

Figure 6(b) Streamline in one cell bounded by
two planar streamlines, *Ra*=1000.

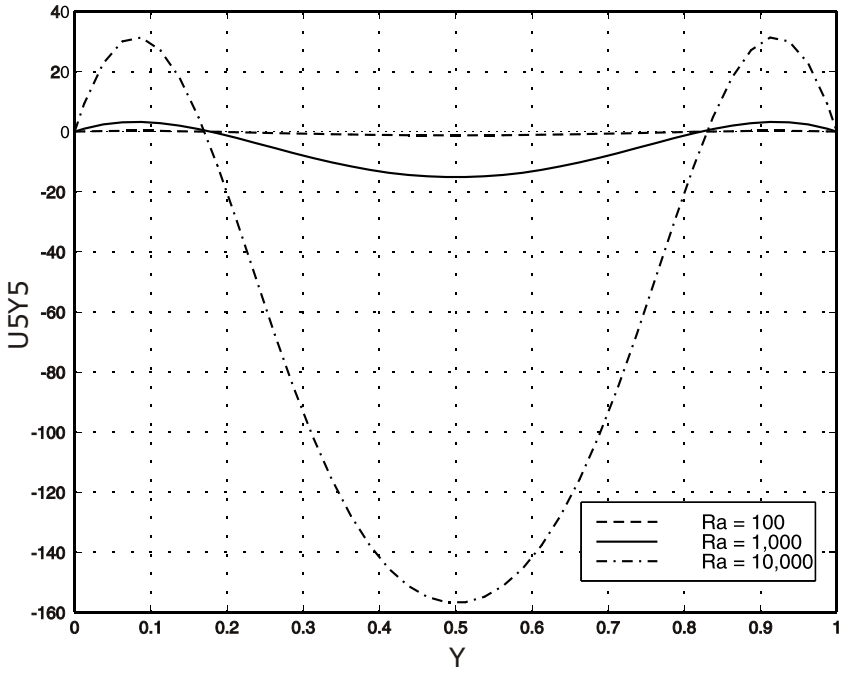

Figure 6(c) *u* velocity on the centreline *x*=*z*=0.5.

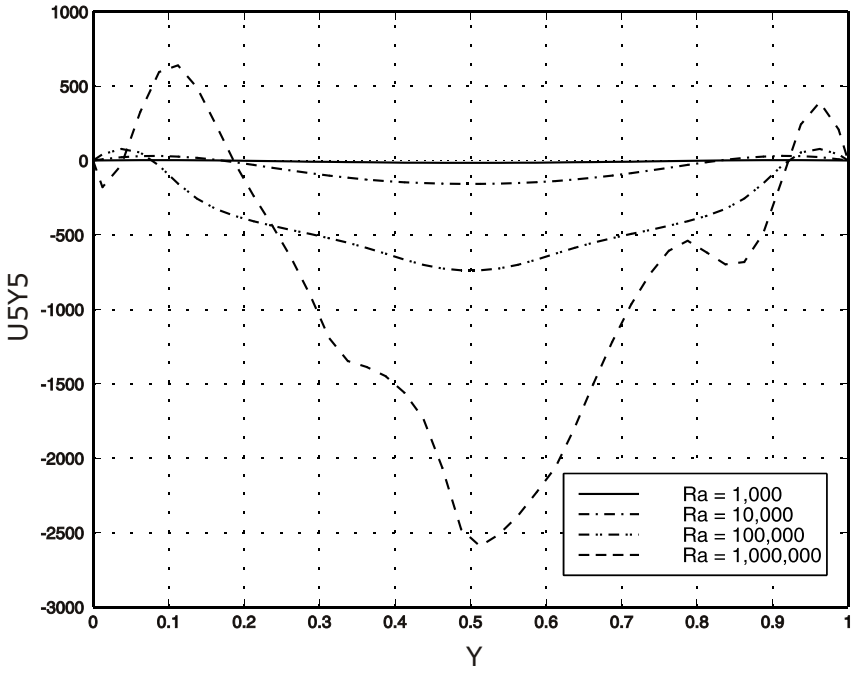

Figure 6(d) *u* velocity on the centreline *x*=*z*=0.5.

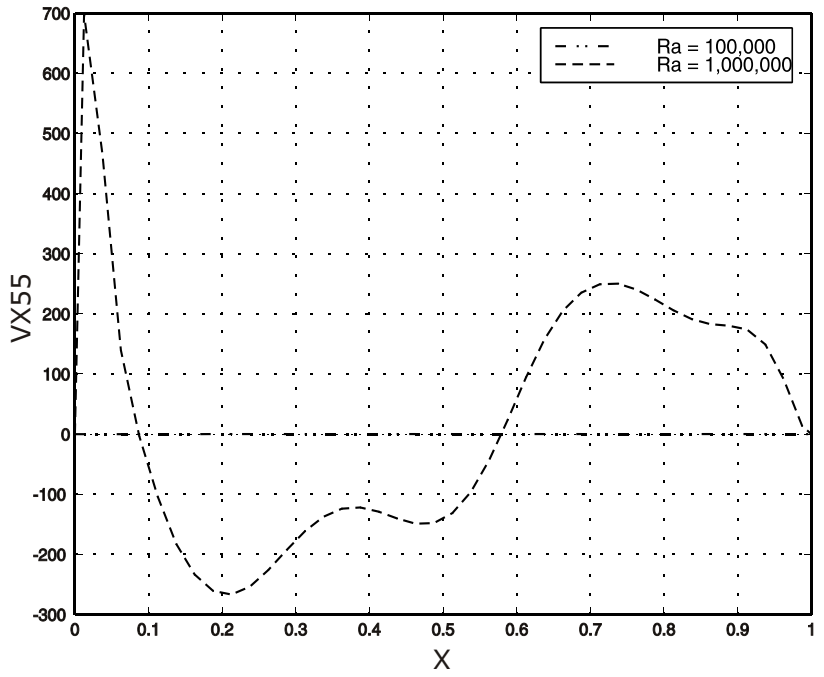

Figure 6(e) *v* velocity on the centreline *y*=*z*=0.5.

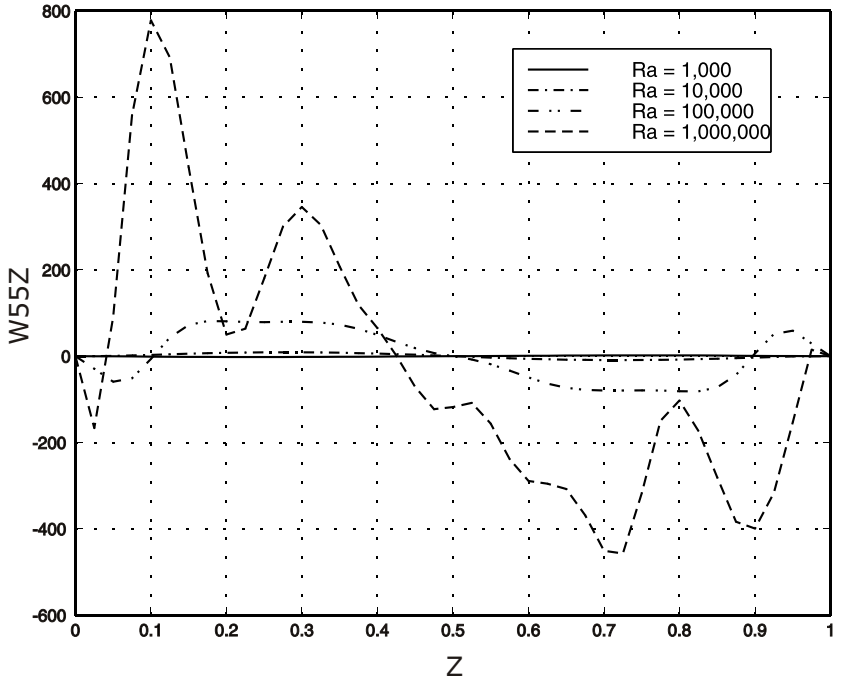

Figure 6(f) *w* velocity on the centreline *x*=*y*=0.5.

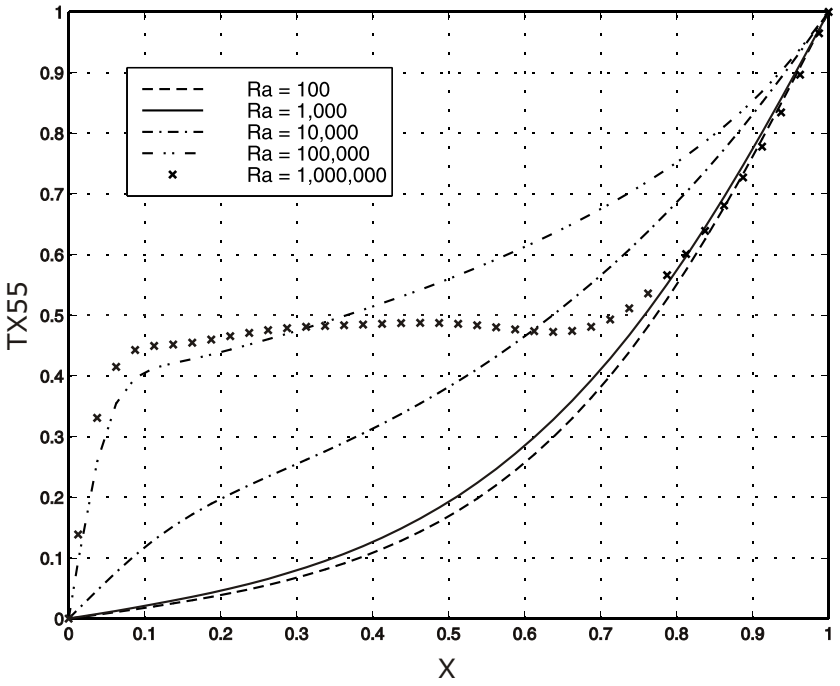

Figure 6(g) Temperature on the centreline $y=z=0.5$. Flow is steady for all values of Ra except $Ra=10^6$.

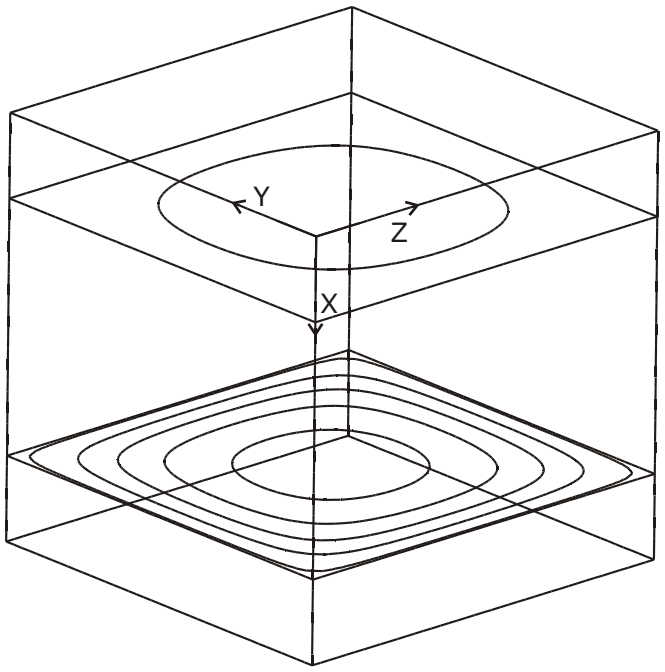

Figure 6(h) Temperature contours on $x=0.2$ and $x=0.8$ planes, $Ra=1000$.

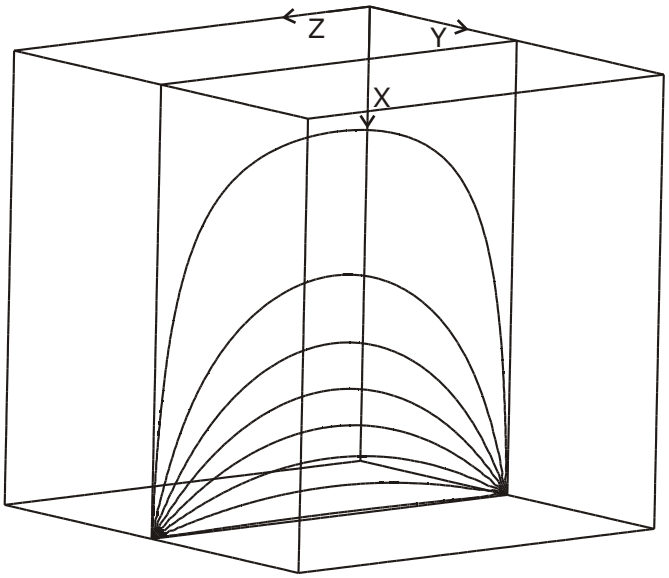

Figure 6(i) Temperature contours on y=0.5 plane, Ra=1000.

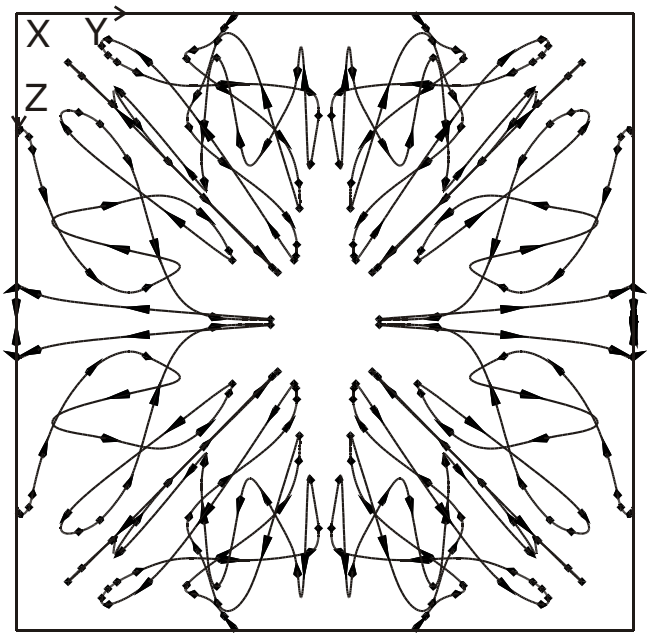

Figure 6(j) Streamlines in top view along x-axis, Ra=10^5.

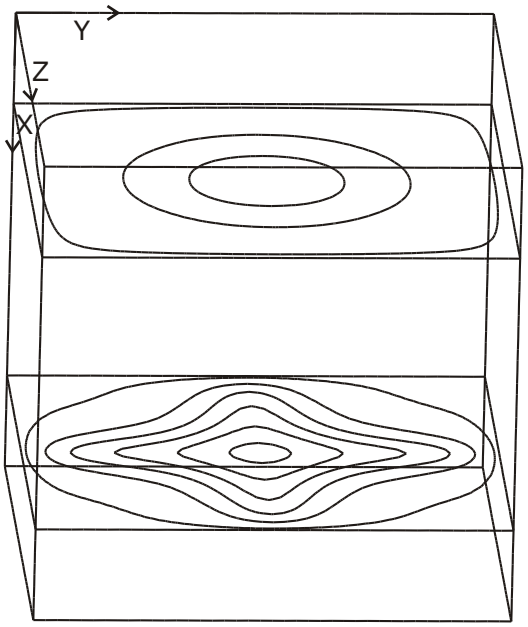

Figure 6(k) Temperature contours on x=0.2 and x=0.8 planes, Ra=10^5.

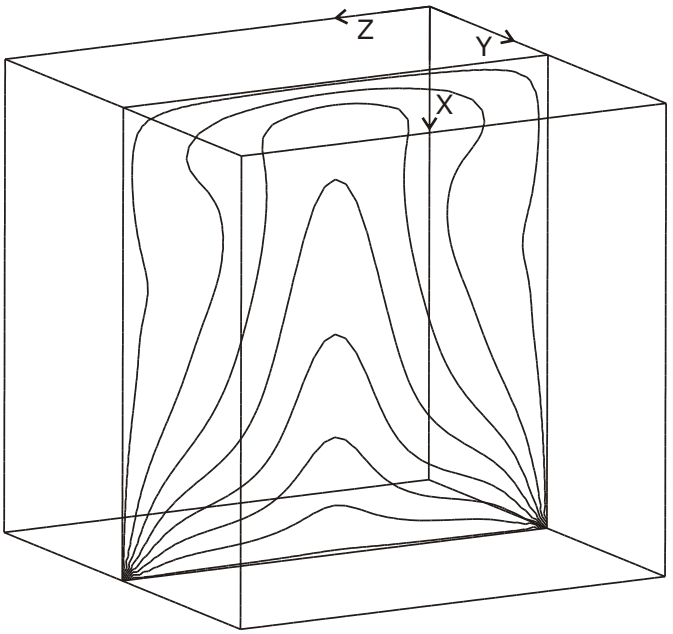

Figure 6(l) Temperature contours on y=0.5 plane, Ra=10^5.

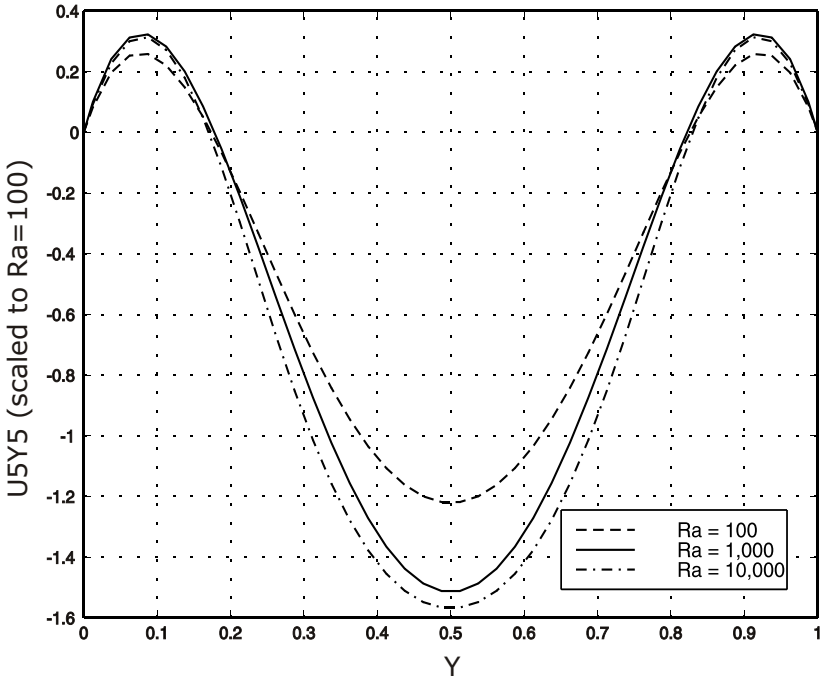

Figure 7. Case C, cubical cavity heated from below.
(a) *u* velocity on the centreline *x*=*z*=0.5 scaled by *Ra* to correspond to *Ra*=100, *Pr*=0.1.

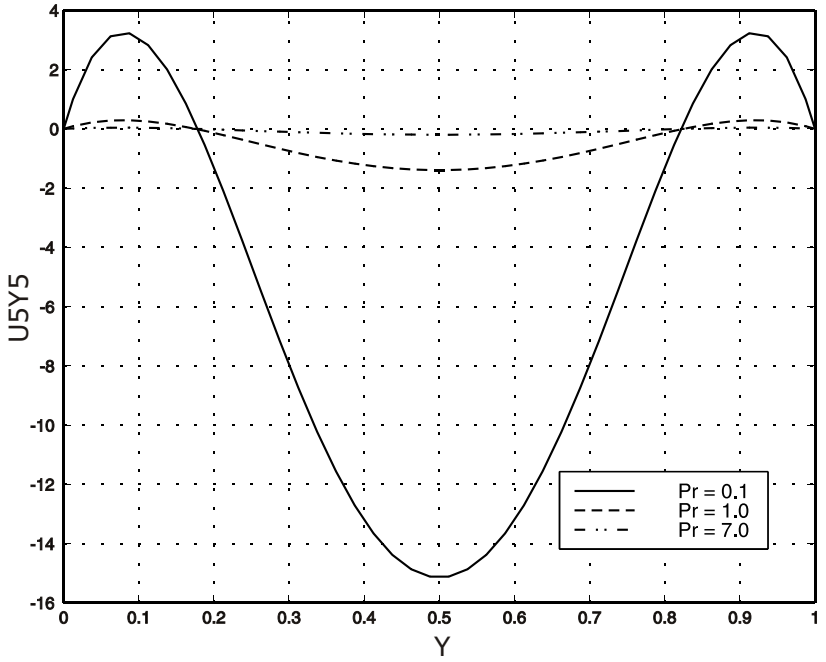

Figure 7(b) *u* velocity on the centreline *x*=*z*=0.5 for *Pr*=0.1, 1 & 7; *Ra*=1000, *Pr*=0.1 .

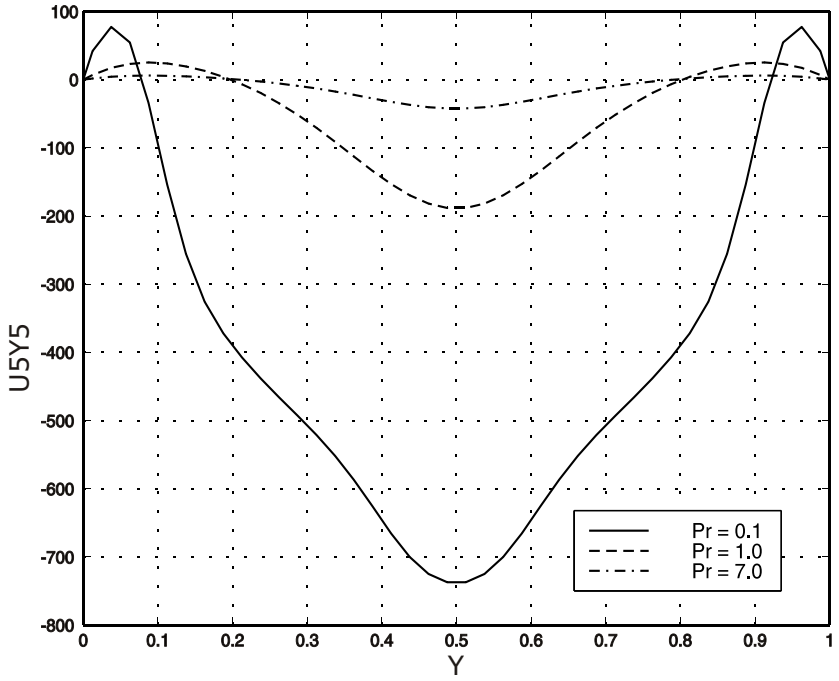

Figure 7(c) *u* velocity on the centreline $x=z=0.5$ for $Pr=0.1$, 1 & 7; $Ra=10^5$.

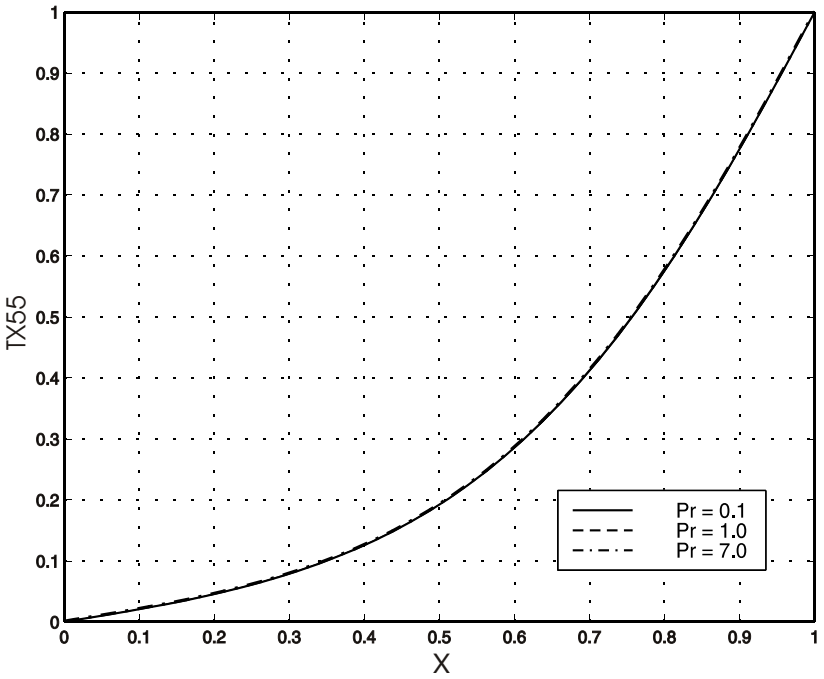

Figure 7(d) Temperature profiles on the centreline $y=z=0.5$ for $Pr=0.1$, 1 & 7; $Ra=1000$.

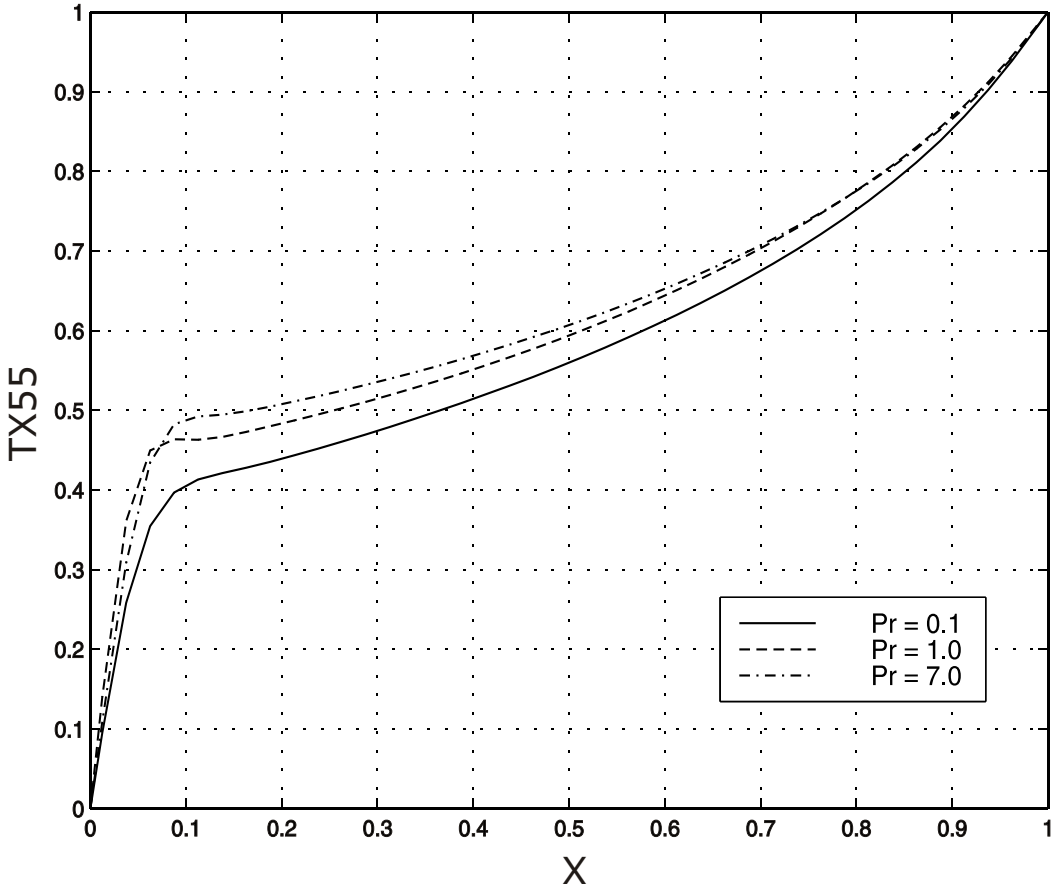

Figure 7(e) Temperature profiles on the centreline $y=z=0.5$ for $Pr=0.1$, 1 & 7; $Ra=10^5$.

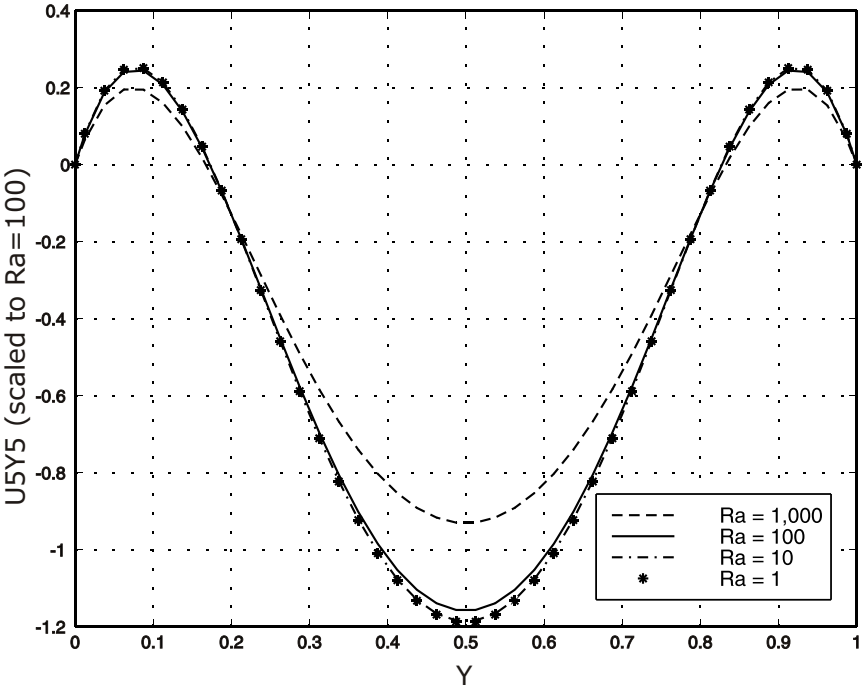

Figure 8. Case D cubical cavity heated from top. *Pr*=0.1. (a) *u* velocity on the centreline *x*=z=0.5 scaled by *Ra* to correspond to *Ra*=100.

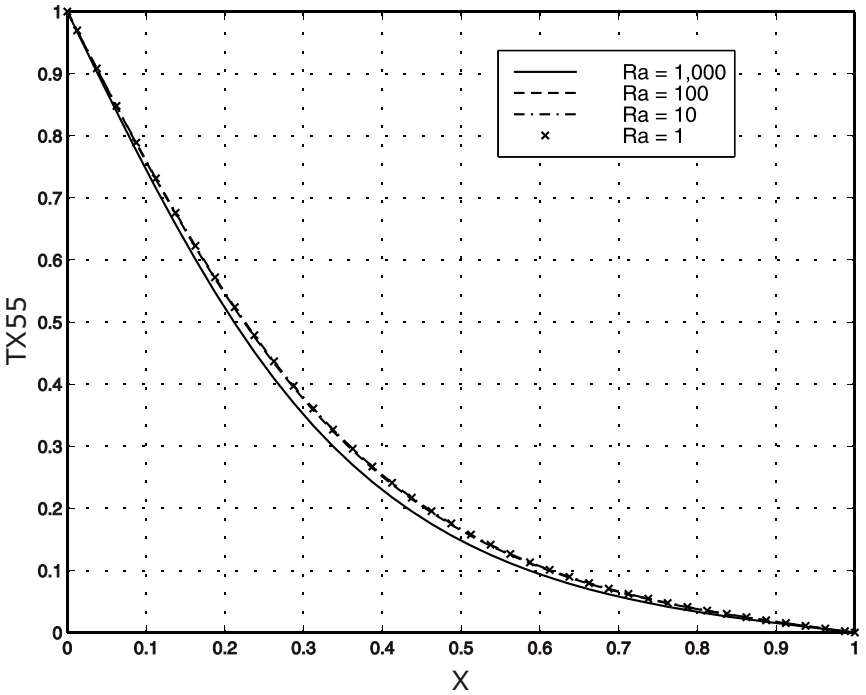

Figure 8(b) Temperature profiles on the centreline *y*=*z*=0.5 for different *Ra*.

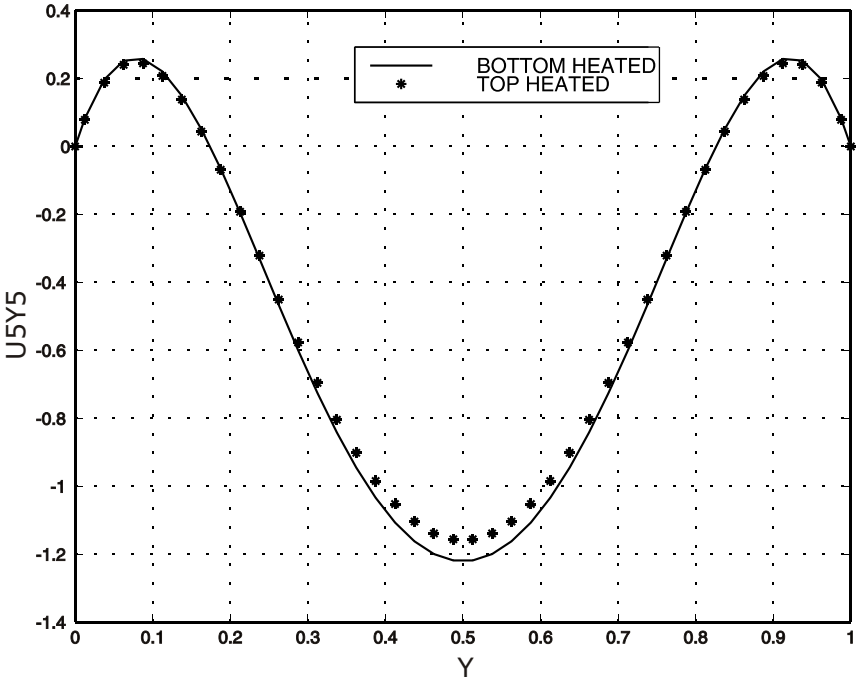

Figure 9. Comparison of cases C and D for *u* velocity on the centreline $x=z=0.5$. $Pr=0.1$. (a) $Ra=100$.

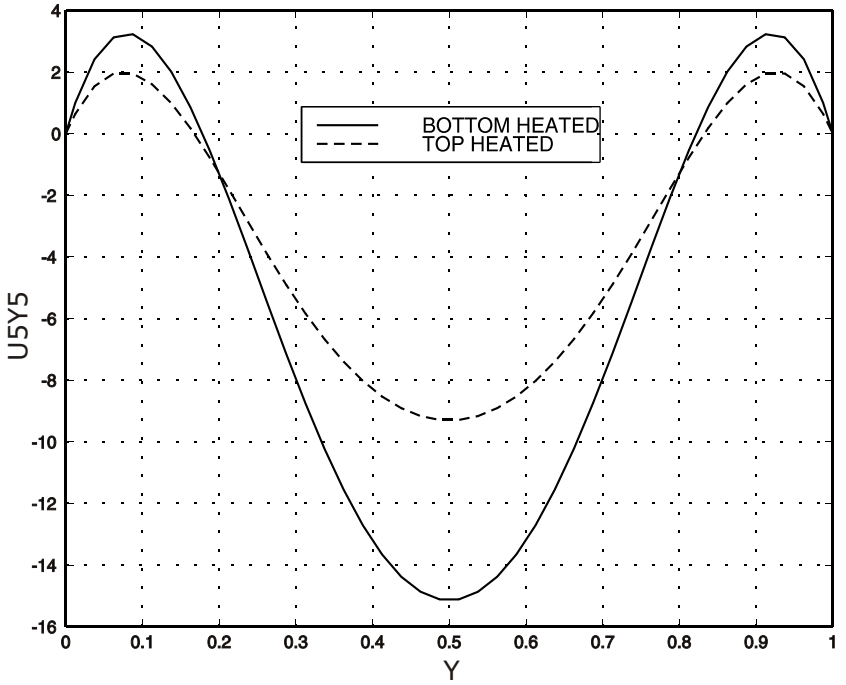

Figure 9(b) $Ra=1000$.

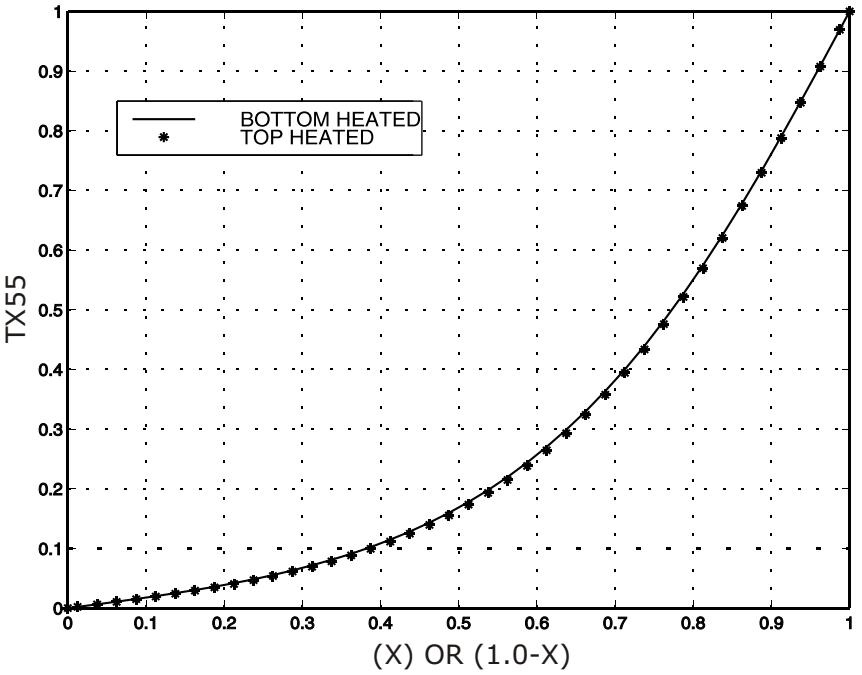

Figure 10. Comparison of cases C and D for temperature profiles on the centreline $y=z=0.5$. $Pr=0.1$. (a) $Ra=100$.

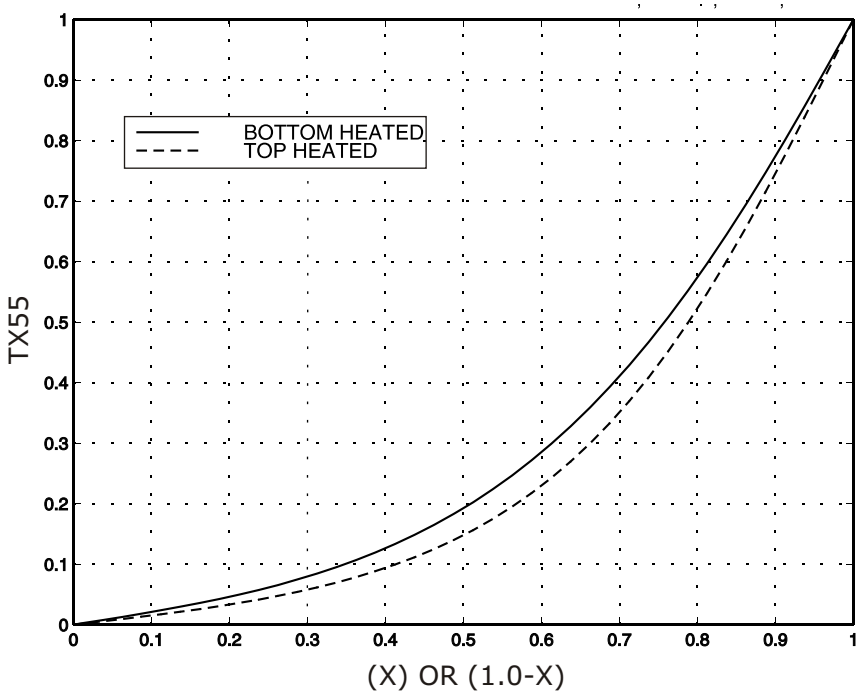

Figure 10(b) $Ra=1000$.

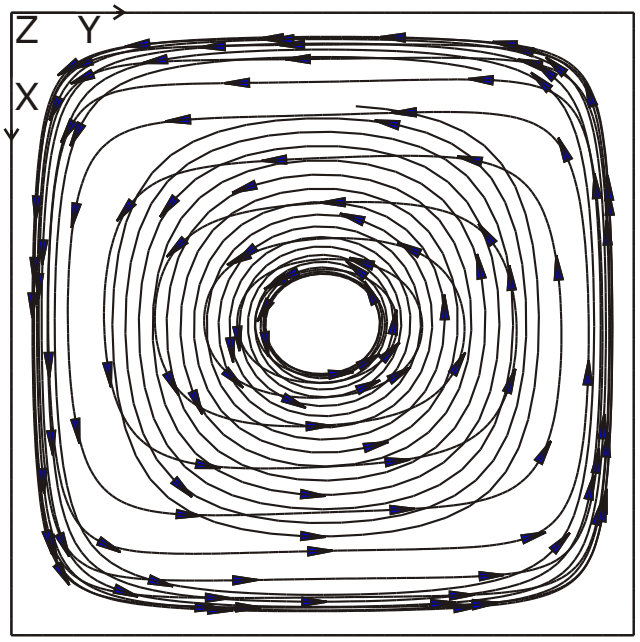

Figure 11. Streamlines in a cubical box heated and cooled symmetrically from sides, case E. (a) *Ra*=100, front view along z-axis.

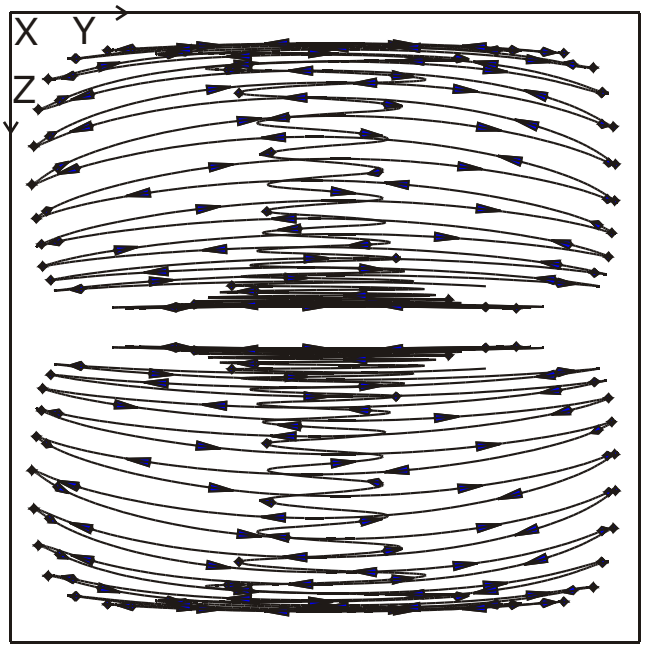

Figure 11(b) *Ra*=100, side view along x-axis.

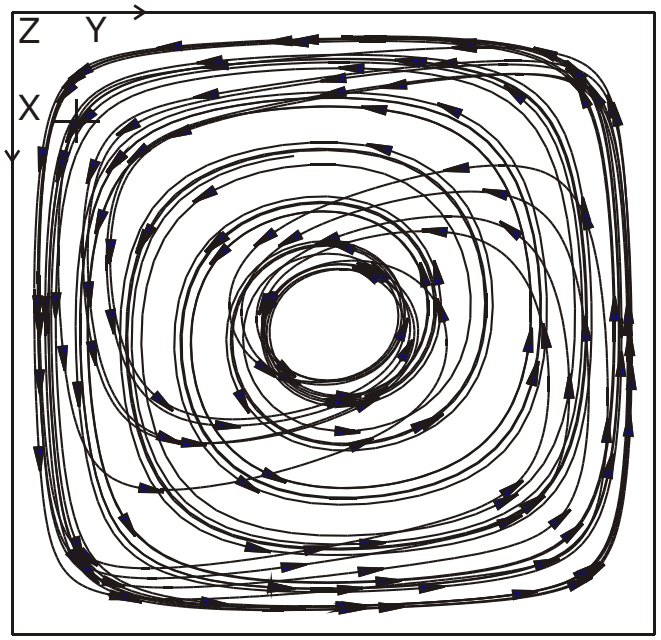

Figure 11(c) *Ra*=1000, front view.

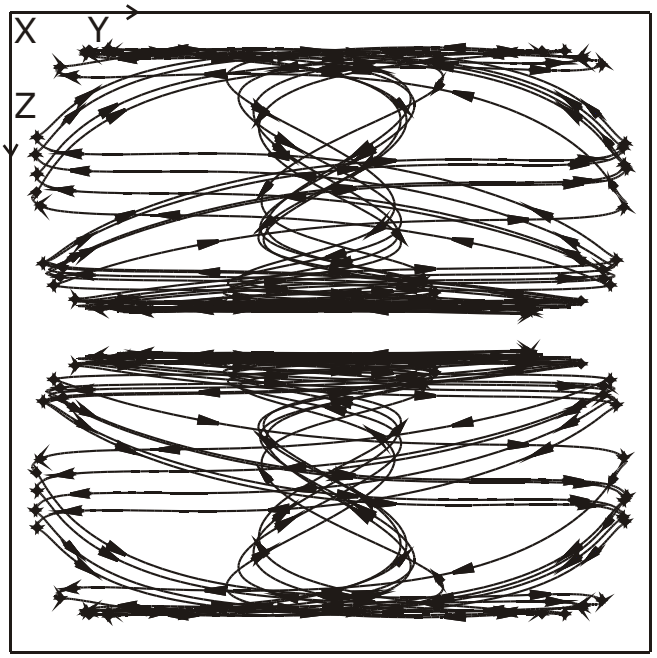

Figure 11(d) *Ra*=1000, side view.

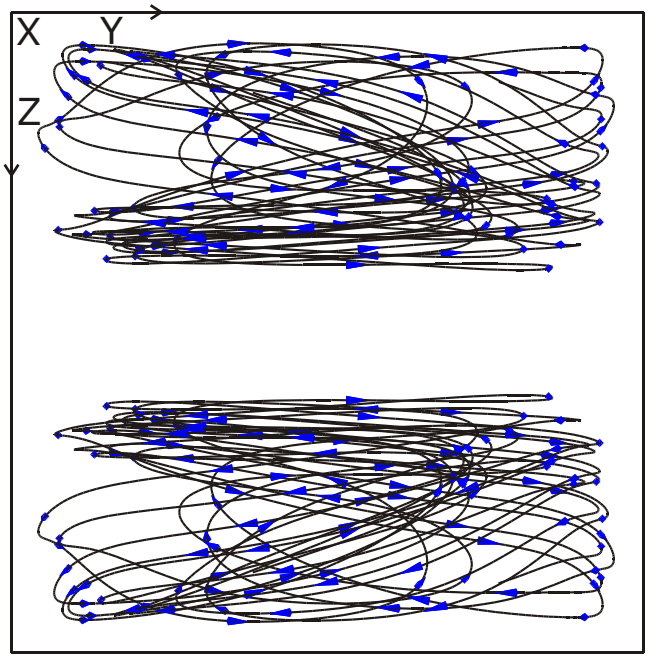

Figure 11(e) *Ra*=10,000, side view.

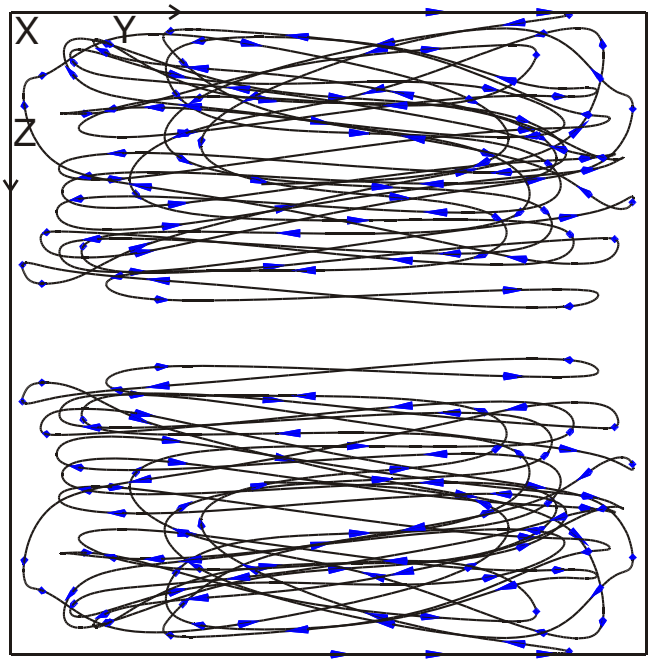

Figure 11(f) *Ra*=10^5, side view.

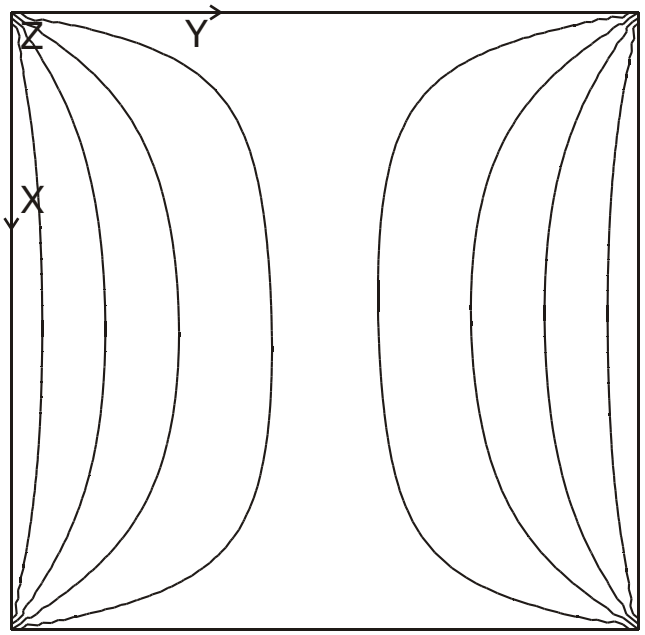

Figure 12. Temperature contours in z=0.5 plane for a cubical box heated and cooled symmetrically from sides, Case E. Pr=0.1. (a) Ra=100.

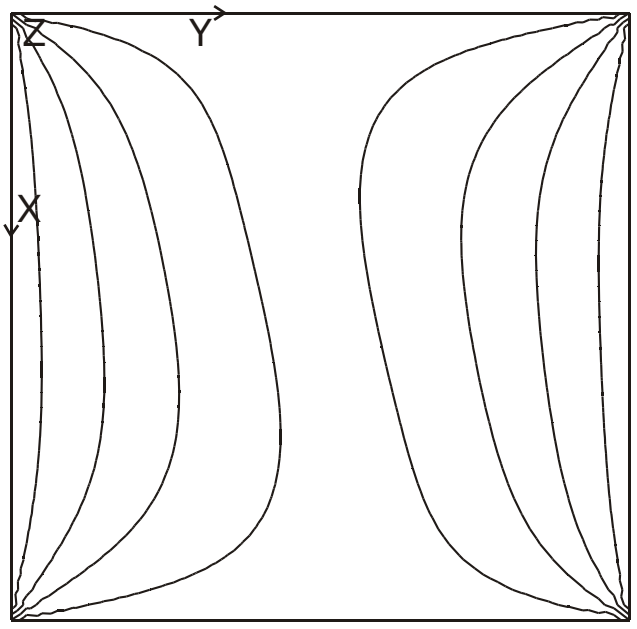

Figure 12(b) Ra=1,000.

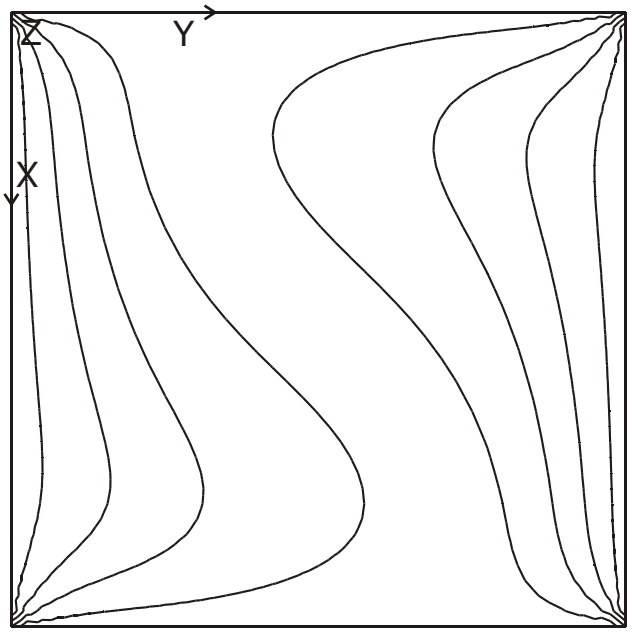

Figure 12(c) *Ra*=10,000.

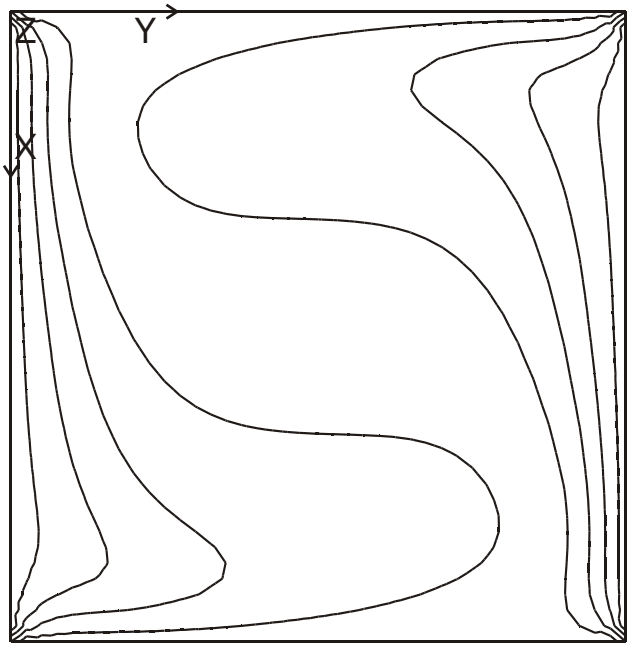

Figure 12(d) *Ra*=100,000.

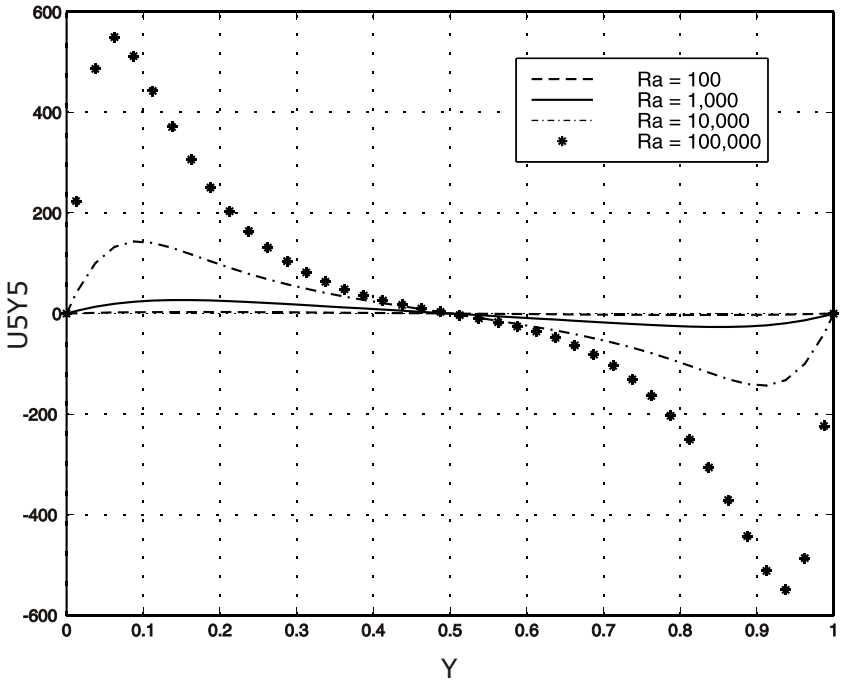

Figure 13. Profiles for a cubical box heated and cooled symmetrically from sides, Case E. *Pr*=0.1. (a) *u* velocity on the centreline *x*=*z*=0.5.

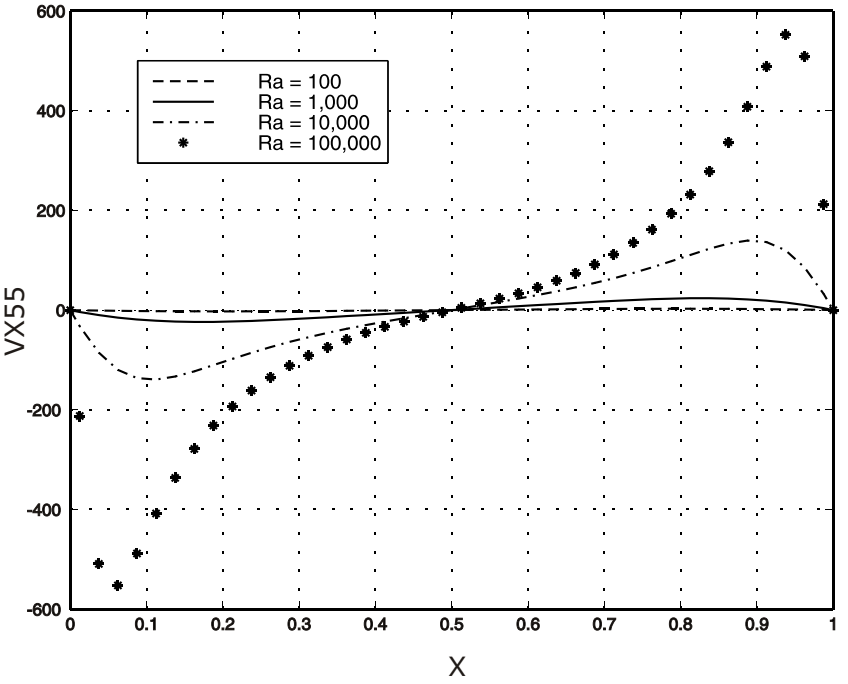

Figure 13(b) *v* velocity on the centreline *y*=*z*=0.5.

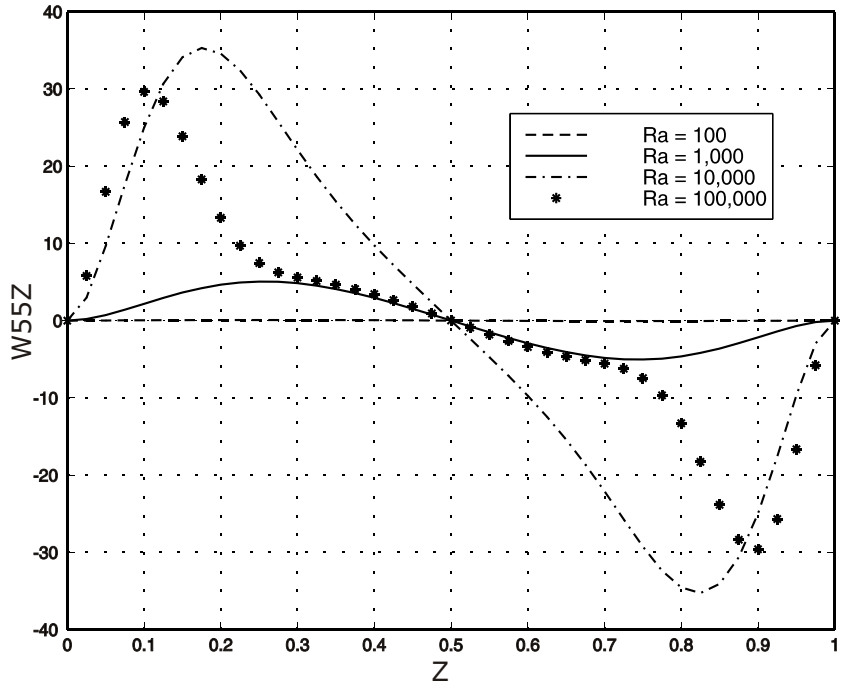

Figure 13(c) *w* velocity on the centreline *x*=*y*=0.5.

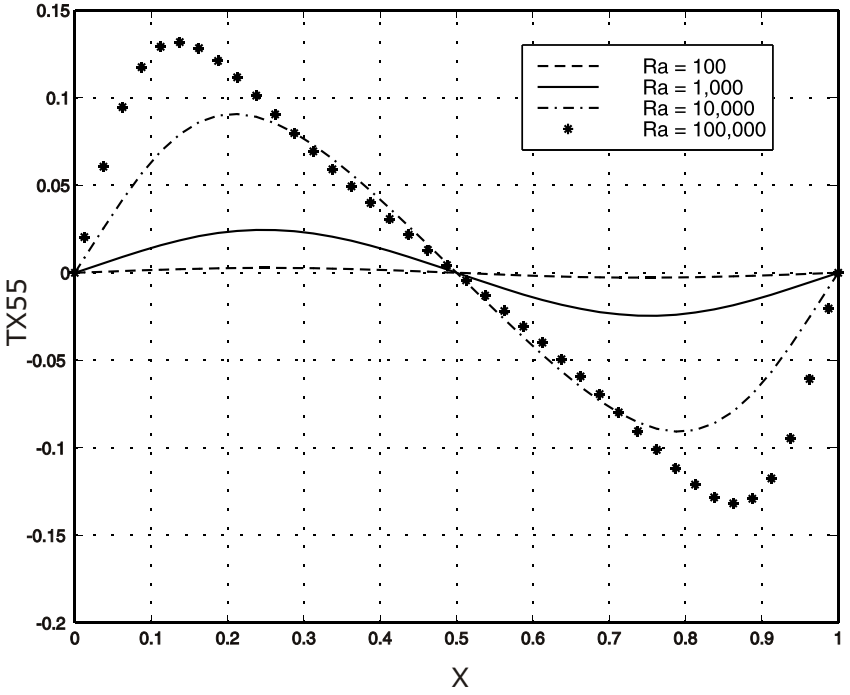

Figure 13(d) Temperature profile on the centreline *y*=*z*=0.5.